Chapter 1

Introduction

1.1. Materials science

Materials science, also referred as materials science and engineering, is an interdisciplinary study concerned with the development of novel materials. The investigations of materials using the materials model (synthesis, structure, characteristics, and performance) are part of this relatively new scientific subject. It is at the forefront of study into nanoscience and nanotechnology and involves components of physics and chemistry. As a distinct branch of science and engineering, materials science has gained popularity recently. A substance (often a solid, but other condensed phases may be included) is characterized as a material if it is intended to be utilized for a certain purpose. We are surrounded by a variety of materials, which are used in everything from spacecraft to structures. Crystalline and non-crystalline materials can often be separated into two categories. Metals, ceramics, and polymers are the classic examples of materials. Semiconductors, nanomaterials, biomaterials, other novel and cutting-edge materials are now being developed. Since then, the field has expanded to encompass all classes of materials, including ceramics, polymers, semiconductors, magnetic materials, materials for medical implants, biological materials, and nanomaterials. We equate ages with materials because they are so crucial to the growth of civilization. In the Stone Age, when humans first appeared on the planet, only organic materials like stone, clay, skins, and wood were used. As a result, one of the most significant interdisciplinary fields in science and engineering that is utilised and applied in daily life, is materials science.

- **Nanoscience**: Study of all types of nanostructures, including their characteristics and processes occurring at the nanoscale (1 nm = 10^{-9} m).

- **Nanotechnology**: the attempt to control and manipulate the studies of nanostructures in order to find various applications for them.

1.2. Classifications of nanostructured materials (low dimensional systems)

The materials with nanostructures are divided into various groups in nanotechnology (Figure 1.1). The dimensionality of nanostructured materials is a crucial factor in their classification. The classification of the nanostructured materials into the following groups was based on their decreased dimensions to the nanoscale range (100 nm):

Zero dimensional (0-D) systems – All three dimensions—length, breadth, and height—are at the nanoscale level in zero-dimensional systems. Charge carriers like electrons or holes are constrained in all three dimensions and are unable to travel freely in any direction in these systems. Single crystal, polycrystalline, and amorphous particles with all-viable morphologies akin to spheres, cubes, and platelets are all included in zero-dimensional systems. Quantum dot is an example.

- **One dimensional (1-D) systems** – One dimension in these systems is macroscale, whereas the other two dimensions are nanoscale. In one dimension, the electrons or holes are free to move while being constrained in the other two. Quantum wire is an example of this type of system.

- **Two dimensional (2-D) systems**– These systems have two macroscale dimensions and one nanoscale dimension. The charge carriers can move freely in two dimensions but are constrained in one. Quantum well is an example of this type of system.

- **Three dimensional (3-D) systems** – In these systems, there are no nanoscale dimensions and all three dimensions are macroscale. Charge carriers are free to move in all three dimensions of three-dimensional systems. Bulk material is an example.

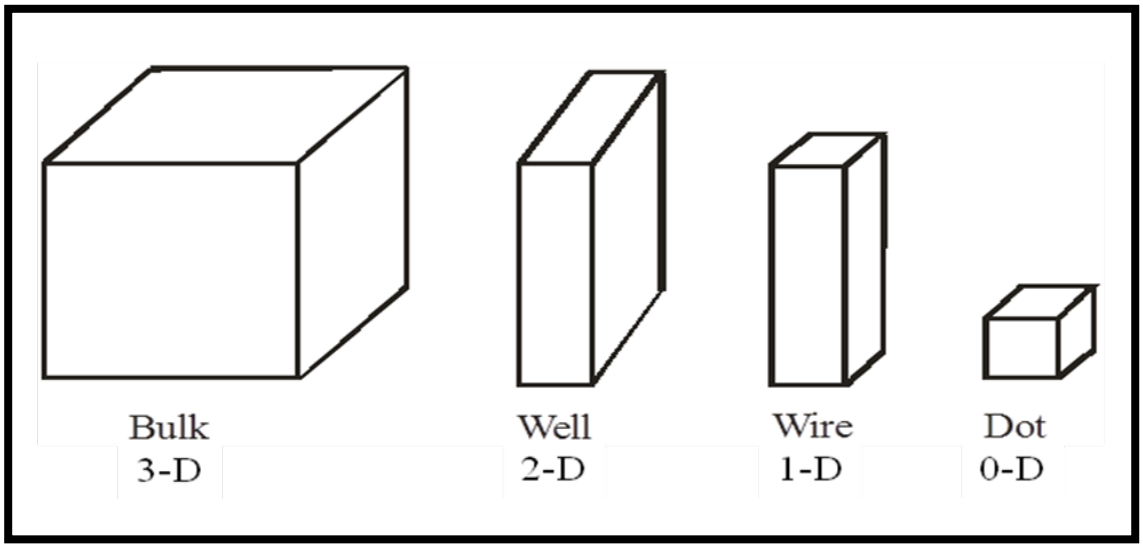

Figure 1.1. Schematic presentation of reduced-dimensional systems

Particles with at least one dimension in the nano range (1 to 100 nm) are referred to as nanoparticles. These particles are extremely reactive due to their large surface area and dense surface charge. Between bulk materials and atomic or molecular structures, nanoparticles serve as a bridge [1]. The main distinction between these two types of materials is that although nanostructures have size-dependent physical properties, bulk materials have constant physical properties regardless of size. Due to this, when nanoparticles get smaller and more atoms are found on the surface of materials, their characteristics alter [2].

1.3. Metal oxides and mixed metal oxides nanoparticles

Metal oxides and mixed metal oxides are known for their diverse applications in human life among the various sorts of materials. Due to their intriguing features, metal oxides are particularly important in many fields of chemistry, physics, biology, and materials science [3][4],[5]. The metal elements can use a variety of synthetic techniques to create a wide range of oxide compounds. These can adopt a huge variety of structural geometries with electronic structures that can have characteristics of insulator, semiconductor, or metallic materials. A novel set of physical and chemical properties that are wholly distinct from those of the individual constituents may be obtained when two or more metal oxides are mixed together either by physical or by chemical methods to fabricate mixed metal oxide nanoparticles [6].The unique characteristics of nanomaterials are caused by surface effects, quantum tunnelling effects, and quantum size effects [7, 8, 9].Due to the emergence of quantum size effects, the confinement of carriers like electrons or holes in low dimensional systems or nanostructured materials may cause a significant alteration in their physical and chemical properties. When at least one dimension of the material is similar to the particle's de Broglie wavelength, the confinement or quantum size result becomes significant [10]. The Schrödinger wave equation provides a quantitative understanding of many features of nanostructured materials or low dimensional systems by predicting physical properties of materials at nanoscale size in formulations of quantum mechanics. Any quantum system in which the charge carriers are free to travel in one, two, or zero dimensions is referred to be a low dimensional or confined system. The carrier energy states and density of states become quantized in these systems because the spatial dimensions are of the order of the de Broglie

wavelength of the carriers. Therefore, quantum-mechanical principles regulate how the carriers behave in the areas of electrical, electronics, chemistry, magnetics, and optics. According to these principles, all matter at the nanoscale exhibits both wavelike and particle like behavior [11]. A wave function is adequate to explain a particle or system of particles and provides all the information about a physical entity, such as an electron, hole, or photon, or even a physical system, such as an atom.

Metal oxides and mixed metal oxides nanoparticles have been made into nanomaterials in a variety of morphologies, including nanorods [12], nanowires [13], nanospheres [14], nanosheets, nanoplates, nanocubes [15], nanofibers [16], flower-like nano granules [17], [18], [19], hierarchical nanostructures [20], nanoribbons [21], nanoflakes, and nanotubes [22]. The content, particle size, surface area, shape, structure, crystallinity, homogeneity, and synthesis processes of nanomaterials all affect their physico-chemical properties [23], [24]. There are few examples like Ce_2O_3–TiO_2 composite nanofibers (Figure 1.2) [16], ZnO nanorings (Figure 1.3), NiO nanotubes (Figure 1.4) [22], flower-like CuO (Figure 1. 5) and γ-Fe_2O_3 spherical nanoparticles (Figure 1. 6) [25].

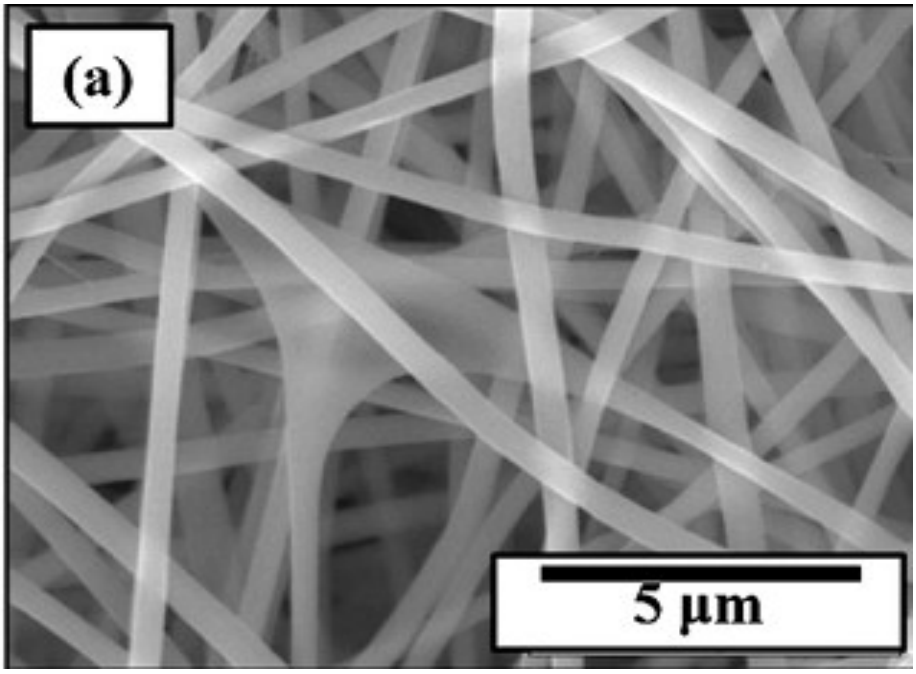

Figure 1.2. SEM image of the Ce_2O_3–TiO_2 composite nanofibers [M.S. Hassan et al. (2012)]

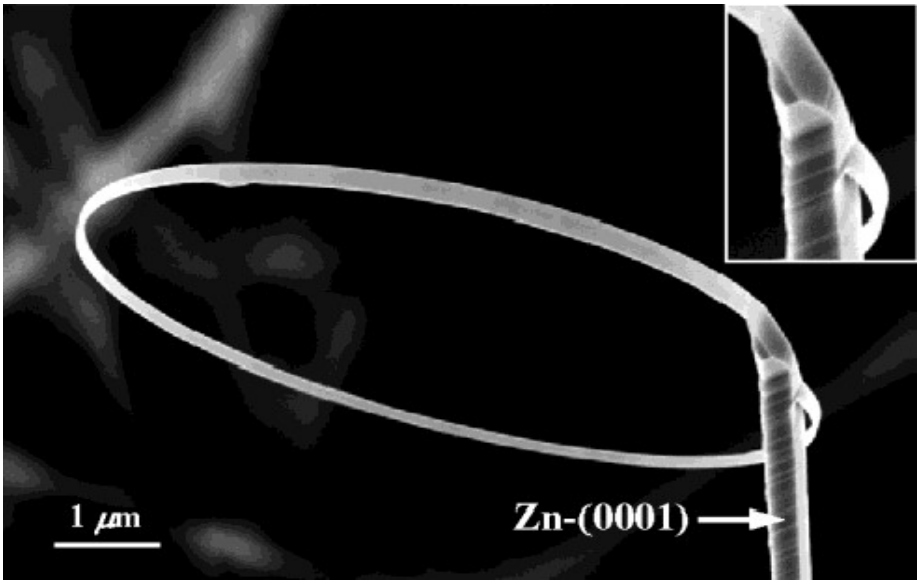

Figure 1.3. SEM image of ZnO nanorings [W.L. Hughes et al. **(2004)]**

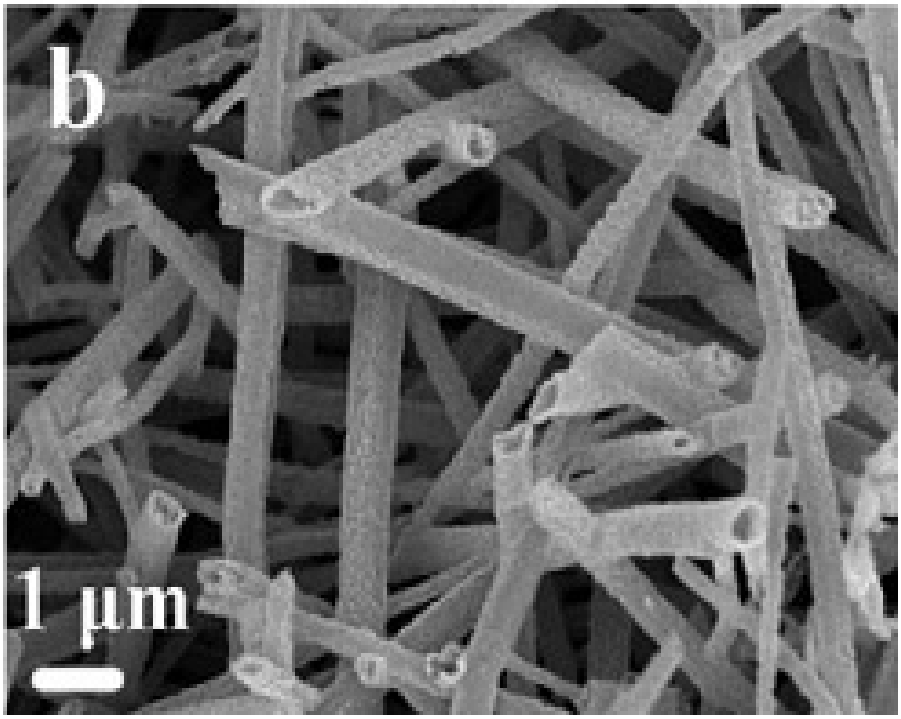

Figure 1.4. SEM image of NiO nanotubes [H. Pang et al. (2009)]

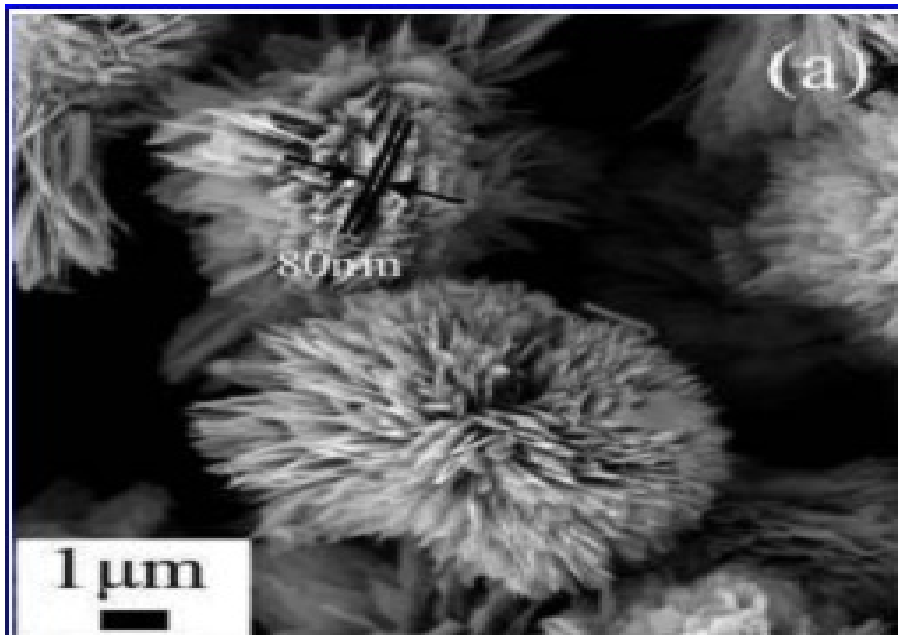

Figure 1.5. SEM image of flower-like CuO [M. Yang et al. (2011)]

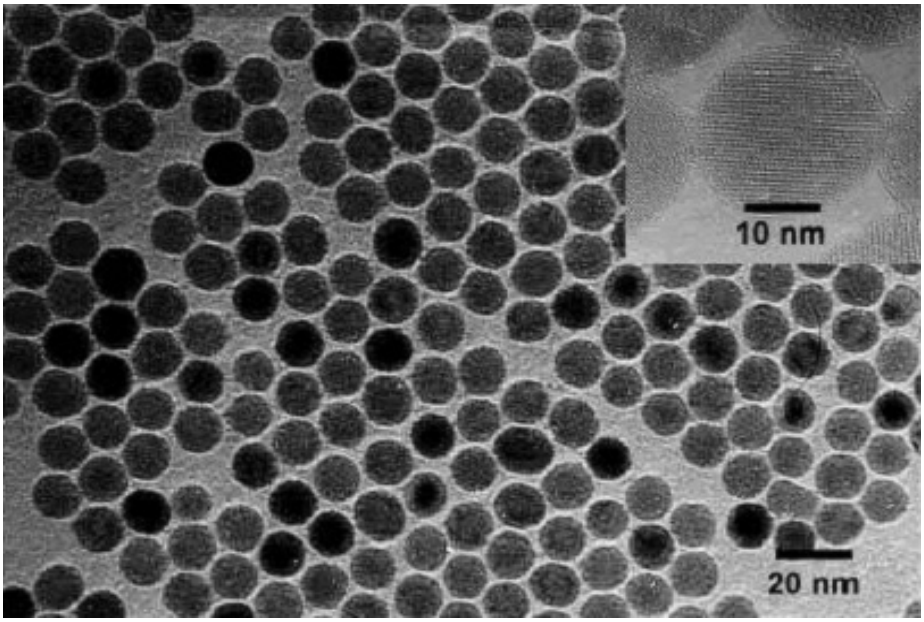

Figure 1.6. TEM image of γ-Fe_2O_3 spherical nanoparticles [T. Hyeon et al. (2001)]

1.4. Applications of metal oxides and mixed metal oxides nanoparticles

Due to their potential applications in many fields, including catalysis [19], photocatalysis [27][28], sensors, antimicrobial activity [30], biomedical [31], electronics [32], optics [33][33],[34],[35], magnetic materials [36], medicines [37], adsorbents [38],[39], UV-blockers and filters [40], fuels cells [41],[42][43], solar cells [44], waste water treatment, [45], Metal oxides and Mixed Metal oxides nanoparticles have received great interest. It have also important applications in biological and medical sciences such as cancer treatments, drug delivery, fluorescent imaging, bio labeling and bio tagging.

- ZnO-Fe_2O_3 nanoparticles have been shown by Gordon et al. to be antibacterial against Staphylococcus aureus and Escherichia coli [31].

- In several chemical processes, such as the Baeyer-Villiger oxidation of cyclohexanone to caprolactone and the oxidation of dimethyl ether to hydrocarbons, SnO_2-MgO nanoparticles operate as catalysts [49].
- At room temperature, CuO-ZnO mixed oxide nanoparticles function as active CO oxidation catalysts [50].
- Many harmful substances, such as acid gases and organophosphorous compounds, can be effectively adsorbed using nanocrystalline MgO [51, 52].
- For hydrogenating benzene, SiO_2-NiO nanoparticles are thought to be the best catalysts [53].
- ZnO nanoparticles have potent antifungal properties against Penicillium expansum and Botrytis cinerea.
- Using TiO_2-ZnO mixed oxides as photocatalysts for hydrogen synthesis from water splitting has been reported [54].
- High surface area, low cost of manufacture, and inherent porosity of NiO nanoparticles make them an ideal adsorbent for removing heavy metals from aqueous solutions [55].
- Nanoparticles of titanium dioxide and zinc oxide are now found in cosmetics, toothpaste, sunscreens, paint, and coatings for vitamin supplements, among other common home items.
- Photocatalytic disinfection of harmful bacteria Staphylococcus aurous and Escherichia coli in water by NiO/$SrBi_2O_4$ under the influence of visible light [56].

- Humidity sensing has been employed using CuO-NiO nanoparticles.
- Co-Cu mixed metal oxide microspheres that have a flower-like hierarchy serve as incredibly effective catalysts for the selective oxidation of ethylbenzene.
- Materials with nanostructures that are utilised in medicine, such as active substances in cancer therapy and drug administration, tissue engineering, fluorescent biological labels, quick tests for medical diagnoses, protein detection, tumour devastation, and separation and purification of biological components and cells.
- Materials with nanostructures are also used in cosmetics, such as tooth paste, UV light protection creams, and antiseptic cream.

These uses have caused research on these kinds of structures to quickly increase.

The development of synthetic processes to regulate nanoparticle shape, morphology, size, and crystallinity is receiving a lot of interest.

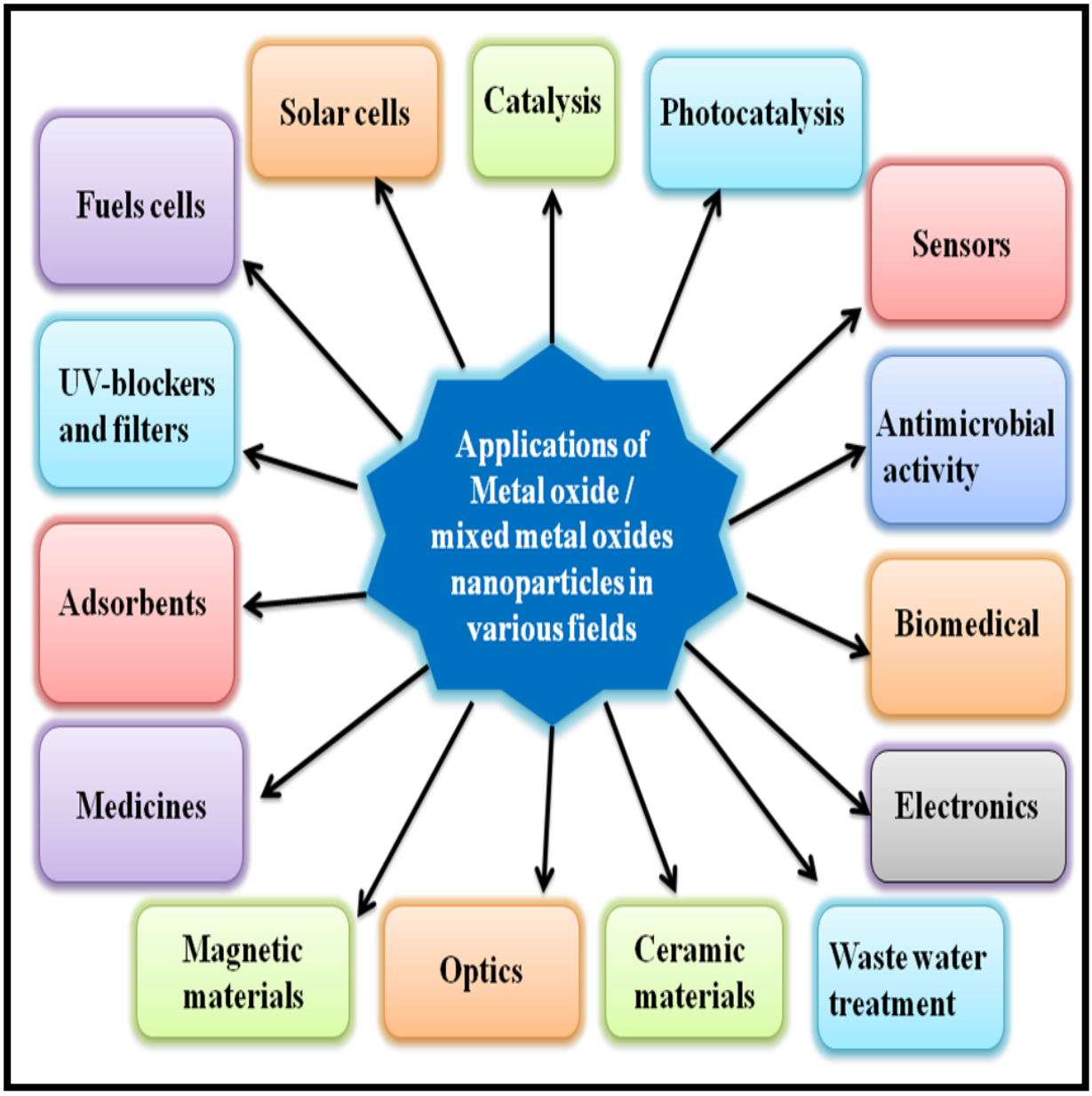

Figure 1.7. Application of metal oxides and mixed metal oxides nanoparticles in various fields

1.5. Perovskite oxides: A General Introduction

Perovskites are materials that share the crystal structure of a natural mineral called calcium titanium oxide ($CaTiO_3$). They were first discovered in the Ural Mountains of Russia in 1839 by Gustav Rose and later named after the Russian mineralogist L. A. Perovski. Perovskite materials exhibit a fundamental composition expressed as ABO_3, wherein A and B correspond to distinct cations, with A being larger in size than B. The anion is symbolized by O. Within perovskite structures, the B ions can encompass transition metal ions sourced from the 3d, 4d, or 5d series, adopting an octahedral coordination pattern. The crystal lattice features the A cations, which are larger, and oxygen atoms arranged in a face-centered cubic (FCC) configuration, constituting a modified version of the perovskite framework. The comparatively smaller B cations occupy the octahedral interstitial gaps within this FCC arrangement. This arrangement is seen in numerous oxides, with some of these compounds holding practical applications. Comprehending the arrangement and interconnection of ions within the perovskite configuration is of paramount importance, as it directly influences the properties requisite for specific applications. Numerous perovskite oxides, along with ceramic oxides featuring elevated dielectric constants, find application in capacitor fabrication. The essential criterion for producing capacitors capable of storing substantial energy revolves around possessing a pronounced dielectric constant while minimizing dielectric loss.

In 1967, Deschanvres et al. discovered a family of compounds known as $ACu_3Ti_4O_{12}$, where A represents Ca, Ba, or Sr. Subsequently, Bochu et al. in 1979 determined the accurate structures of this expanded family. These compounds, referred to as $ACu_3Ti_4O_{12}$ type oxides, possess a complex perovskite structure and are renowned for their high dielectric constant. This property has led to numerous important applications. Currently, capacitor materials such as $BaTiO_3$ or relaxor ferroelectrics like $Pb(Mg_{1/3}Nb_{2/3})O_3$ [PMN], $Pb(Zn_{1/3}Nb_{2/3})O_3$ [PZN], and $Pb_{1-x}La_x(Zr_{1-y}Ti_y)O_3$ [PLZT] (Moulson et al., 2003) are commonly used but are not environmentally friendly despite their high dielectric constants ranging from 1000-20,000. Problem with $BaTiO_3$ is that it is a ferroelectric perovskite which is quite unstable and shows phase transition. Dielectric constant is not stable with temperature (T) and it is not suitable for use at high temperature. High ε_r ferroelectric materials that undergo a phase transition near Curie temperature are not ideal choices. However, a promising alternative is a high ε_r material called Calcium Copper Titanate $CaCu_3Ti_4O_{12}$ (CCTO) belonging to $ACu_3Ti_4O_{12}$ family, and was first discovered by Subramanian et al. and Ramirez et al. in 2000. Based on the previous studies, CCTO exhibits a pseudo-cubic perovskite structure with the space group of Im3 and the lattice parameter of 7.391 Å (Bochu et al. in 1979). It possesses very high dielectric constant ($\sim 10^4$) exhibited by (CCTO), which remains nearly constant in the temperature range of 100 - 600 K. The inherent stability positions of CCTO as a promising material with the potential for numerous significant applications in the fields of microelectronics and memory devices. The static dielectric constant of a material plays a crucial role in determining the extent of miniaturization achievable, making CCTO's stability particularly valuable. The electronic

industry can greatly benefit from the extensive utilization of CCTO in the production of various electronic components. These components include multilayer capacitor (MLCC), dynamic random access memory (DRAMs), microwave devices, as well as electronic devices found in automobiles and aircrafts (Hongtao et al., 2008; Ezhilvalavan et al., 2000; Kretly et al., 2003; Kretly et al., 2004). Despite extensive research efforts encompassing experiments and theoretical investigations, the nature and origin of the colossal dielectric constant observed in CCTO ceramics, continue to be subjects of controversy and unresolved to this day. At present, a possible explanation, an internal grain boundary barrier layer capacitance (IBLC) model at the grain boundaries between semiconducting grains (West et al., 2004; Grubbs et al., 2005) is widely accepted by the researchers. Till date, numerous studies have been conducted to examine the dielectric properties of both CCTO ceramics and single crystal, along with other related materials. The high loss tangent (tan δ) of the CCTO ceramics (tan $\delta > 0.05$ at 1 kHz) is still the most serious problem for applications based on capacitive components. Hence, there is a strong demand for lead free-dielectric materials that exhibit high dielectric constant, low tangent loss (tan δ) and excellent stability across a wide range of temperatures and frequencies. Several researchers (Jha et al., 2003; Jin et al., 2007; Liu et al., 2006) have explored various methods to achieve the giant dielectric material. However, the traditional solid state reaction method, though widely adopted, suffers from issues of precursor material homogeneity. Consequently, this approach requires higher sintering temperatures and longer sintering times for solid state diffusion to promote single phase-formation. To overcome these challenges, chemical methods have been sought to improve homogeneity, lower sintering temperatures, and

reduce sintering times. Investigating several factors, such as sintering temperature, time, ceramic compositions, processing techniques, and the dielectric and electrical behaviour of CCTO ceramics in response to temperature, is necessary to comprehend and optimise their properties. We report the most recent advancements in CCTO ceramic in this chapter. To create CCTO ceramics with optimised qualities, it is crucial to understand its impact and identify the appropriate processing settings. The impact of various parameters, such as sintering temperature, sintering duration, ceramic compositions, different processing methods, and their electrical behavior dependence on temperature and frequency, etc., is summarised with a view to understanding and improving the dielectric properties. Novel dielectric materials are generating a lot of interest right now. Dielectric materials are a type of substance. The impact of various parameters, such as sintering temperature, sintering duration, ceramic compositions, different processing methods, and their electrical behaviour dependence on temperature and frequency, etc., is summarised with a view to understanding and improving the dielectric properties. Novel dielectric materials are generating a lot of interest right now. Dielectric materials are a type of material that effectively supports an electrostatic field while being a poor electrical conductor. Over time, there has been a persistent need for new, affordable dielectric materials with high dielectric permittivity and extraordinarily low dielectric loss. The development of novel ideas, concepts, and designs for incorporating these materials into microwave devices and structures, ensuring maximum effectiveness and performance, continues to receive a lot of attention. The development of a special dielectric ceramic substrate required the use of suitable materials and a carefully specified synthesis technique. There has been a lot of interest in materials with a high

dielectric constant of 10^3 or above. One of the main problems influencing the development of ceramic capacitor technology has been the pressing need for ceramic capacitors with high dielectric constants. However, It was not until 1941 that Thurnauer et al. discovered the extraordinary dielectric constant of barium titanate (ε_r = 1,100) that high ε_r dielectrics (materials with dielectric constants higher than 1000) achieved their most significant breakthrough. However, the temperature-dependent nature of the dielectric permittivity of barium titanate has raised concerns about its widespread use in electronic industries (Kay et al., 1949; Jaffe et al., 1971). As a result, scientists and technologists are actively engaged in seeking alternatives that exhibit thermally stable high ε_r (relative permittivity) and maintain a constant value over a wide frequency range of 10^4-10^6 Hz between 100-600 K. Perovskites have emerged as promising candidates, displaying the desired properties mentioned above. Due to their importance for fundamental research and their high potential for technological applications, such as superconductivity, insulator-metal transition, ionic conduction characteristics, dielectric properties, and ferroelectricity, these oxides have been the subject of extensive investigation since 1940 [57][58],[59]. Perovskites are essential for chemically modifying composition and structure, and as a result, they display a variety of physical and chemical behaviors that are important for industry and depend on processing settings, oxygen content, and ordering [60][61][62][63]. The extensive spectrum of structure-dependent electrical, magnetic, optical, and catalytic capabilities that they possess make them unique as well. [64][65][66][67]. These materials can be classified as insulators, semiconductors, or even metals with superconducting properties [68][68],[69][70],[71]. The fact that the perovskite structure is universal is evidence of its enormous structural and

compositional flexibility. Perovskite oxides must be designed to be close to a tolerable instability, whether it be of structural, electronic, or magnetic origin, in order to be functionally useful [63],[72],[73]. Titanate perovskite is of tremendous interest because of its unusual electrochemical properties, thermoelectric and ferroelectric capabilities, and industrial usage as electrodes, transistors, and memory. The alkaline earth metal titanate was composed of $BaTiO_3$, $SrTiO_3$, $CaTiO_3$, and its associated non-stoichiometric complexes. (Ca, Sr, Ba) TiO_3, which are important ferroelectric materials, are the perovskite-type materials that have received the most attention and are employed the most. $SrTiO_3$, $CaTiO_3$, and $BaTiO_3$ are ferroelectric and quantum paraelectric, respectively. It has been shown that the structural flexibility of perovskite can produce or enhance desirable solid-state properties, such as ionic or electronic conductivity. [74]. The titanium-based oxides, a member of the well-known perovskite family, are also becoming more well-known due to their potential uses in nonlinear optics, gas detection, and other fields. Due to its high permittivity, low dielectric loss, and dielectric behaviours, $BaTiO_3$ is commonly utilised as an insulating material in electronic ceramic producers while $CaTiO_3$ is frequently employed as a wireless device [75]. On the other hand, $SrTiO_3$ has garnered a lot of theoretical and experimental interest for its defect chemistry and radiation resistance [76][77][78]. Today, it is possible to alter the electrical and physico-chemical properties of perovskites by introducing flaws and impurities into their structural makeup, as well as order-disorder effects. [79], [80], [81]. The features of these perovskite oxide can be changed to create a brand-new system with entirely original characteristics. Extensive experimental and theoretical research on perovskite-based materials over the past ten years has shown a strong

correlation between distortions of the crystal structure and a variety of processes and phenomena, including photoluminescence, ferroelectric, piezoelectric, and pyroelectric properties [82], [83], [84], [85].

1.6. Classification of Perovskite

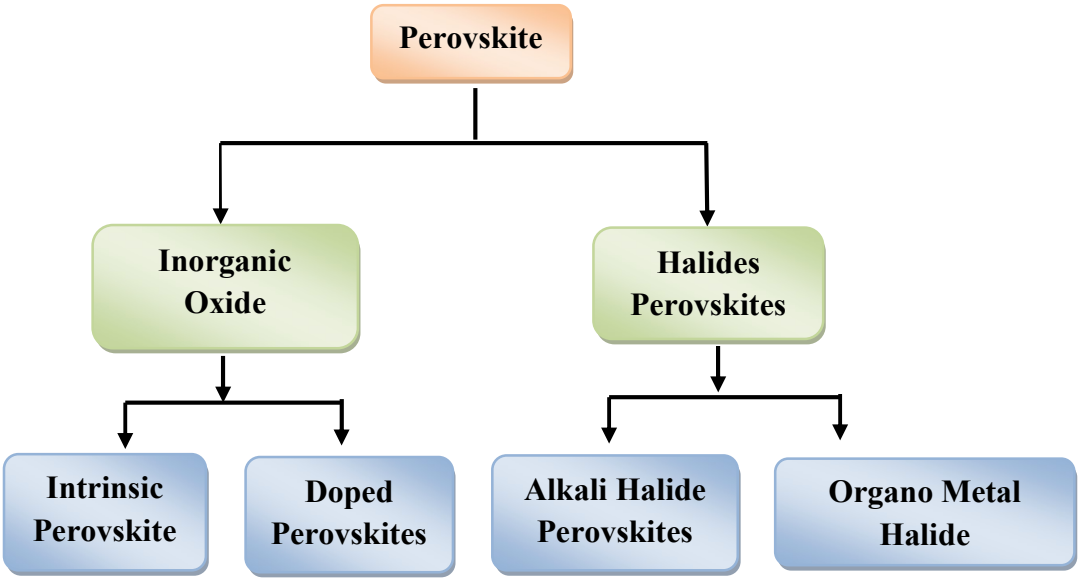

Fig. 1.8. Classification of perovskite

1.7. Type and Structures of Perovskite

a. ABO_3 Perovskite: The perovskite structure has the chemical formula ABO_3, where A and B stand for two distinct cations. Eight BO_6 octahedral are surrounded by twelve 12-fold coordination sites, and it is made up of BO_6 octahedral joined to one another by corner oxygen [85]. Because the A and B ions have distinct ionic radii, the existence of two different size cation sites allows for a wide range of perovskite-type oxides. Because of its unique electrical and photo-catalytic characteristics, perovskite oxides are constantly the centre of attention.[86],[87][88] and some example of perovskite used for ionic

conductivity, ferromagnetic and piezoelectric i;e. $BaTiO_3$, $PdTiO_3$,$SrTiO_3$ and $CaTiO_3$ etc [89]. Additionally, perovskites have structural flexibility with reference to cation and anion vacancies. Goldschmidt postulated a tolerance factor (t) based on this connection, which deviates from the optimum ratio of the ionic radii. (equation 1.1).

$$t = \frac{r_A + r_O}{\sqrt{2}(r_B + r_{O)}} \qquad (1.1)$$

where, respectively, r_A, r_B, and r_O present ionic radaii of A, B, and O ions. When the tolerance factor (t) is 1, a cubic structure is visible. If t is less than 1, however, the A cation is too tiny to form a cubic structure, which causes the BO_6 octahedral network to bend and reduce the A cation site's available space. Perovskite compounds are typically found in the 0:75 < t < 1 range and cubic-type forms when t > 0.9.

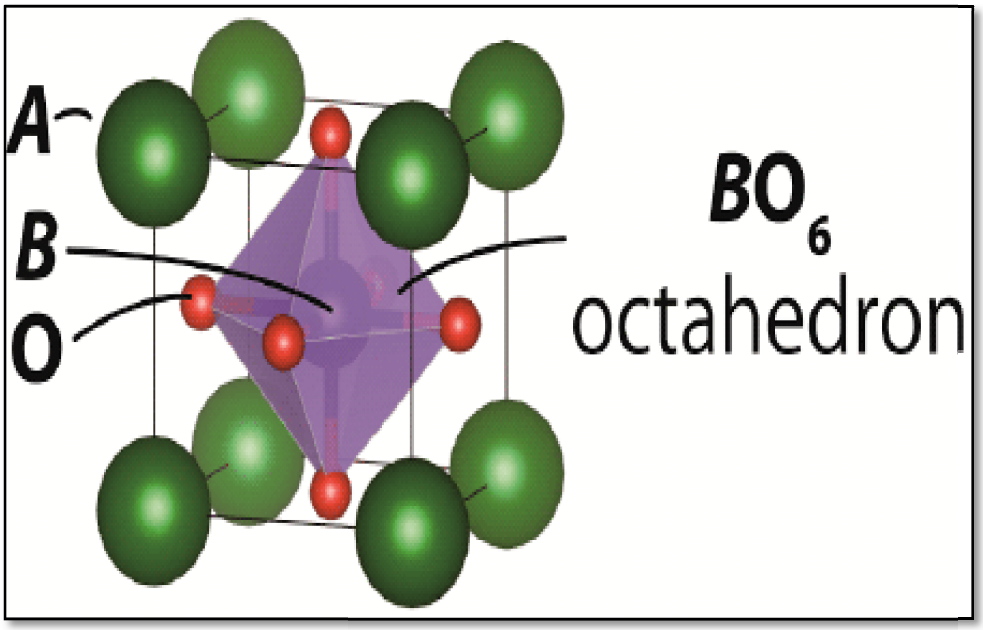

Fig.1.9. The structure of ABO_3 perovskite [79]

b. **$A^{+1}B^{+5}O_3$ Perovskite:** Perovskites with $A^{+1}B^{+5}O_3$ include $LiNbO_3$, $KNbO_3$, $AgNbO_3$, $NaNbO_3$, and $KNbO_3$. Cation A represents the first group element of the periodic table, while Cation B represents the fourth group element. Both ferromagnetic and antiferromagnetic characteristics can be seen in these materials [90]. One of them, $NaNbO_3$, has an orthorhombic unit cell and is an anti-ferromagnetic at room temperature. However, as the temperature rises, the structure of the material changes, displaying cubic structure at 693 K, pseudo-tetragonal structure at 833 K, and tetragonal structure at 913 K. Common electro-optics equipment generally uses these perovskite materials.

c. **$A^{+2}B^{+4}O_3$ Perovskite:** A cation is a member of the second group of the periodic table, where as B cation is a member of the fourth group, making $A^{+2}B^{+4}O_3$ type of perovskite, which is the most popularly utilised in dielectric and piezoelectric materials. The majority of A and B are present in tetravalent (Ti, Zr, and Sn) and divalent (Ca, Sr, and Ba) ions. One of these well researched perovskite materials is $ATiO_3$, where A = Ba, Bi, Ca, La, and Pb. Additionally, piezoelectric and dielectric materials were employed. Perovskite materials made of $BaTiO_3$ and $CaTiO_3$ are suitable for a wide range of applications, including immobilising high-level radioactive waste, transducers, gas lighter elements and piezoelectric materials [91].

d. **$A^{+3}B^{+3}O_3$ Perovskite:** This type of compounds belonging to rare earth or yttrium ion on A site and a trivalent transition metal ion on B site. The particular interest of these compounds found to be technical application of functional materials and most interest

properties such as mixed conductivity by both ions and electron or hole migrations .Such materials can be employed in a solid electrolyte fuel cell (SOFC) as electrode materials for oxygen sensors and humidity sensors.

e. $(ABO_3)_n$ AO Perovskite: Ruddlesden and Popper have Mentioned a family of perovskite oxide with the general formula $A_{n+1}B_nO_{3n+1}$($(ABO_3)_nAO$), where, n is the number of ABO_3 perovskite layers separated by sole of AO rock salt layer [92]. A and B show the rare or alkaline earth elements. It belonging to R-P homologous series, and most of used for the high oxide-ionic conductivity, R–P homologous materials with mixed ionic electronic conductors for electrodes in intermediate temperature solid oxide fuel cells [93][94],[92].

Materials with a structure similar to K_2NiF_4 have drawn the most attention for the R-P oxides' potential application as electrodes in intermediate temperature solid oxide fuel cells. Due to oxygen interstitial migration in the rock-salt type layers of the structure, K_2NiF_4 type materials exhibit better ionic conductivity than anion deficient ones [95][96]. Additionally, these materials' oxide-ion migration is significantly influenced by octahedral rotation aberrations [97].

f. $A_2B_2O_5$ Perovskite: Numerous materials that display an anion deficient perovskite (oxygen deficient perovskite) ABO_3-system have the general formula $A_2B_2O_5$. The brownmillerite, which gave rise to several derivatives, including layered double perovskites, is thought to be the parent structure of A_2B_2O5 ($A_2BB'O_5$). Perovskites and compounds that resemble perovskite oxides having crystallographic shear planes with site anion and anion vacancy orders. $ABO_{2.5}$ (also known as A_2B_2O5, $A_2BB'O_5$, and $AA'B_2O_5$) is likely the most

well-known and has the greatest structural variety of all the anion deficient perovskites. They are attractive materials for a variety of applications due to their high Curie temperature (Tc), superconductivity in Cu-based oxides, strong electron and oxygen ion conductivity, and rich magnetic behaviour. Best materials are $Ca_2Mn_2O_5$ and $Ba_2In_2O_5$ as oxygen deficient perovskite. According to figure 1.3, the orthorhombic structure of $Ca_2Mn_2O_5$ consists of five coordinated square pyramid subunits between manganese and oxygen, where each of the five oxygen atoms is connected to a neighbouring subunit through a corner oxygen atom.

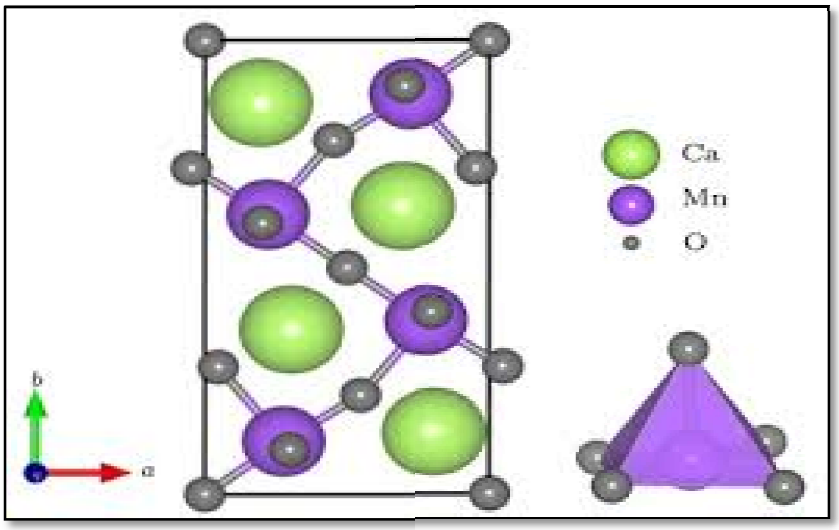

Fig.1.10. Structure of $Ca_2Mn_2O_5$ unit cell showing oxygen vacancy along the direction of normal A B plane.[98]

The six coordinated octahedral subunits of the orthorhombic CaMnO3 are connected by the six oxygen atoms at the corner positions. As a result, the oxygen-deficient locations of the

oxygen-deficient perovskite $Ca_2Mn_2O_5$ exhibit intrinsic molecular level porosity, which is distinct from structural porosity like mesoporosity or macro-porosity [85]

Table 1.1. Example of some perovskite explaining Typical property application and their use.

Compounds	**Typical property**	**Application**	**Used**
$BaTiO_3$, $PdTiO_3$	Ferromagnetic property Piezoelectricity and high dielectric constant.	Multilayer ceramic capacitors (MLCCs), PTCR resistors and embedded capacitance.	Most widely used dielectric ceramic T_C = 125°C
(Ba, Sr)TiO_3, (Bi, Na)TiO_3	Non-Linear dielectric properties.	Tunable microwave devices.	Used in the para-electric state.
Pb (Zr, Ti)O_3	Ferromagnetic property Piezoelectricity.	Piezoelectric transducers actuators and ferroelectric memories.	PZT most successful piezoelectric material.
$Bi_4Ti_3O_{12}$	Ferroelectric with high Curie temperature.	High-temperature actuators and Ferroelectric Properties.	Aurivillius compound T_C = 675°C

$(K_{0.5}Na_{0.5})NbO_3$, $Na_{0.5}Bi_{0.5}TiO_3$	Ferromagnetic property Piezoelectricity.	Lead-free piezo-ceramics.	Performances not yet comparable to PZT but rapid progress.
$SrFeO_3$, $LaCoO_3$	Electrical conductivity.	Alternative dielectric materials and Internal barrier layer capacitors.	Multifunctional material.
$BiFeO_3$, $LaMnO_3$	Magnetic property.	Magnetic field detectors, Memories.	Most investigated multi ferroic compound. T_C = 850°C
$LaCoO_3$, $BaCuO_3$	Catalytic property.	Cathode material in SOFCs and oxygen separation membranes.	Used for Solid Oxide Fuel Cells cathodes.
$LaAlO_3$, $YAlO_3$	Host materials for rare-earth luminescent ions	Lasers Substrates for epitaxial film deposition.	

1.8. Complex Perovskite

Due to the configurationally and chemically ductility of the perovskite octahedral texture, the complex perovskite $(AA)(BB)O_3$ type structure are well supported in various technological applications. Although other compositions also consolidate trivalent rare earth, cation A with charge reveals divalent species in these structures. By combining trivalent species like Al^{+3}, Ti^{+3}, and Fe^{+3} simultaneously on the B site, for example $(Ca_{1-x}Nd_x)$ $(Ti1_{-x}Al_x)O_3$ and $(Pb_{1-x}Ba_x)$ $(Fe_{1-x}Ti_x)O_3$, indemnity is granted. Due to the significant size and charge differences between A and B cations, symmetry might be compromised and several properties, including magnetic and dielectric behaviour, can alter. The perovskite structure explains a lot about the control capabilities and allows for excellent latitude in chemical replacements on both cations. Perovskite A_3BX and BAX_3 extra ingredients inverse perovskite structure are belong to homologus series, such as $A_{n+1}B_nO_{3n+1}$ (Ruddlesden-Popper) [99], $A_nB_nO_{3n+1}$ (Dion-Jacobson) [100], $Bi_2A_{n-1}B_nO_{3n+3}$ (Aurivillius series) [B. Aurivillius(1949), B. Aurivillius(1950), B. Aurivillius (1951)]. An anion deficient perovskite with multifaceted features, such as $A_nB_nO_{3n-2}$ and its relation to ABO_3 perovskite, was described by the structures of several homologous series perovskite oxide. Many of the applications and characteristics of pervoskite, such as ferroelectrics, ionic conductors, superconductors, multiferroics, and magneto resistant materials, were explained by Ruddlesden-Popper and Dion-Jacobson as the result of a complex interaction between the crystal structure, electronic state of the transition metal, degree of defects, and their mutual interaction. Few example of complex perovskite oxides are $CaCu_3Ti_4O_{12}$ (CCTO),

$Bi_{2/3}Cu_3Ti_4O_{12}$ (BCTO), $Y_{2/3}Cu_3Ti_4O_{12}$ (YCTO) and $La_{2/3}Cu_3Ti_4O_{12}$ (LCTO) etc.

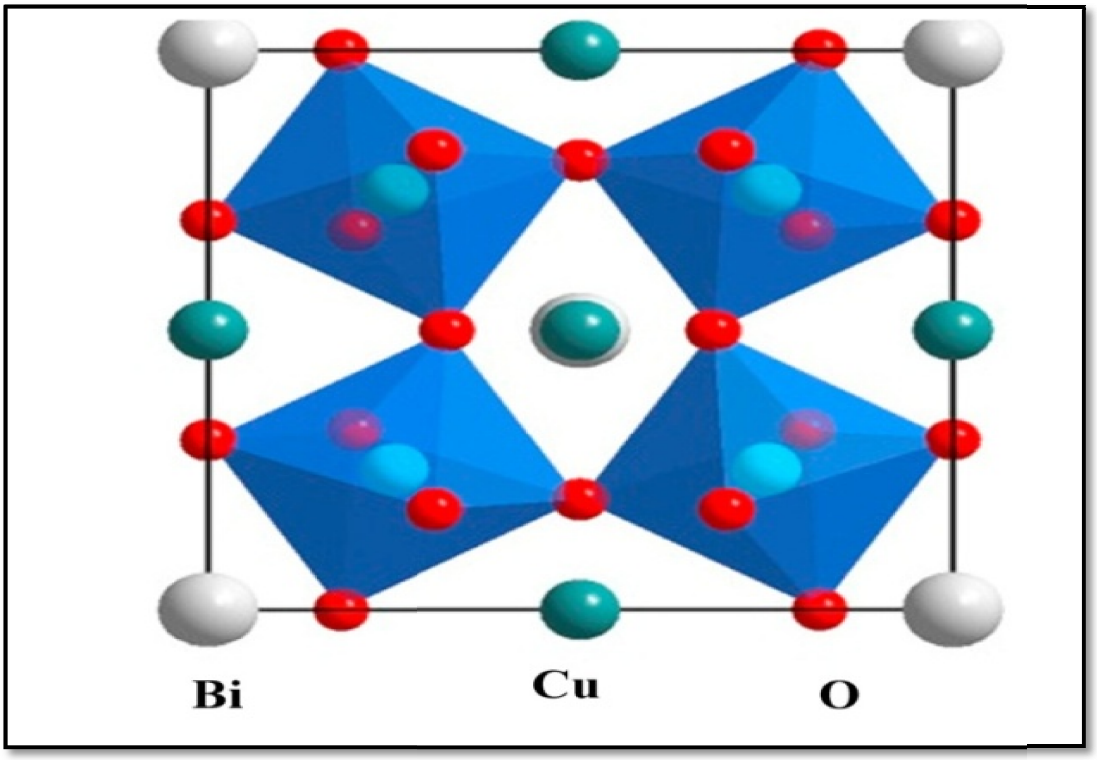

Fig.1.11. Crystal structure of $Bi_{2/3}Cu_3Ti_4O_{12}$ (BCTO) [101]**.**

The cubic structure of the $Bi_{2/3}Cu_3Ti_4O_{12}$ complex perovskite is depicted in Figure 1.11; their space group is Im3 and their lattice constant is 7.413 A°. In this arrangement, charge neutralism is achieved by leaving 1/3 of the Bi sites empty. This could have an impact on the dielectric behaviour, making the investigation of this chemical more intriguing. Similar to the complex perovskite's CCTO structure is the BCTO structure.

1.9. Substitutions in Perovskite: Because they have high dielectric constants, perovskite-structured oxides are highly stabilized and have a wide range of technological uses

(Fouskova et al., 1970). In addition to their doping with various cations changing their characteristics, perovskites are technologically significant materials even in their undoped state (Shao et al., 2007; Rai et al., 2009; Prakash et al., 2006; Patterson et al., 2005; Parkash et al., 2008; Mandal et al., 2009; Li et al., 2006)). The two types of general doping are interstitial and substitution. Due to the tightly packed structure of perovskites, interstitial replacement is challenging. A or B site of perovskites can be substituted with a lot of flexibility, and characteristics of ABO_3 can be changed to make it useful. The following factors, which affect the substitution modifications:

a) Size: The condition is considered favourable when the difference in size between two ions is less than 15%.

b) Chemical Affinity: The solid solubility of the two crystalline minerals will be limited to a greater extent if they exhibit higher chemical reactivity.

c) Structure: Complete solid solubility requires that the two end members possess an identical crystal structure.

d) Valency: Substitution is limited when the introduced ion possesses a valency from the host ion.

The substitution in perovskite oxides can be of the following types:

i) Heterovalent substitution

ii) Isovalent substitution

iii) Valence compensated substitution

(i) Heterovalent substitution:

The valencies of the substituent ion and the ion being replaced differ. To compensate for the extra cost incurred by this substitution, a defective structure will be formed. The substitute can be accommodated at either site A or site B. This substitution is of two types:

(a) Acceptors substitutions: Acceptor impurities are impurities with a lower valency than the cation that replace cations in solid compounds. This either results in holes or oxygen vacancies because the substituent ion it replaces provides less electrons. e.g. substitution of Na^{+} on Ba^{2+} and Co^{3+} on Ti^{4+} site in $BaTiO_3$.

(b) Donors substitutions: A positive ion known as a donor is employed to swap out a lower valency ion on the A or B site. Charge compensation requires a species with an effective negative charge since the impurity has an effective positive charge in comparison to the host oxide's lattice. e.g. electrons or cation vacancy e.g. La^{3+} or Y^{3+} on Ba^{2+} (Zhi et al., 1999) and Nb^{5+} on Ti^{4+} site in barium titanate separately.

(ii) Isovalent substitution: The substituent ion and the ion it replaces share the same valency in isovalent replacements. This substitution may occur on either site A or site B, or both sites concurrently. In $BaTiO_3$,substitutions of Ca, Sr or Pb at Ba site are example of isovalent substitution at A site whereas replacement of Ti ion by Zr, Sn or Hf ions are examples of B site isovalent substitution.

(iii) Valence Compensated substitution: A donor is a positive ion that is used to replace a lower valency ion on the A or B site. Therefore, the impurity has an effective positive charge as compared to the lattice of host oxide, and charge compensation calls for a species with an effective negative charge. In A, B or O sub-lattices such as $M_{1-x}La_xTi_{1-x}M'_xO_3$ (M = Ca^{2+}, Sr^{2+}, Ba^{2+} or Pb^{2+} and $M' = Co^{3+}$, Ni^{3+}, Fe^{3+} etc.) (Prasad et al., 1988 ; Parkash et al.,

1990 (b); Christopher, 1998). Such solid solutions are known as valence compensated solid solutions (VCSS). e.g., La^{3+} ion on Ba^{2+} site and Co^{3+} on Ti^{4+} site simultaneously in $BaTiO_3$: $Ba_{1-x}La_xTi_{1-x}Co_xO_3$. In this case there is a little chance of defect creation.

1.10. Chemical synthesis routes for ceramic material:

Perovskite oxides are commonly produced by the dry approach or conventional solid-state method. In this technique, a combination of oxides of various cations is ground into a fine powder using a pestle and mortar and a suitable liquid (acetone or ethanol) as intermediates. Before being processed once more into a fine powder, a mixture of dried powders is calcined at a particular temperature for a given period of time. The powder is mixed with the proper quantity of a suitable binder (PVA), which is then pressed into the desired shape. To burn off the binder, the completed product is first progressively heated to a specific temperature. Next, it undergoes an annealing process that involves heating it to a higher temperature for a predetermined period of time. After annealing, the sample is chilled at a regulated rate of cooling. A metal ion diffusion at high temperatures is the final result. This approach requires a lot of effort, a slow reaction time, and warm conditions. Because atomic diffusion is restricted in grains with a diameter less than a micrometre, other secondary phases also form during synthesis. To achieve chemical homogeneity, repeated high-temperature annealing, mixing, and grinding are necessary. This prevents the resulting product from having microlevel chemical uniformity. As opposed to solid state techniques, wet chemical approaches enable atomic level mixing of individual components and produce nanocrystalline structures at much lower temperatures. The synthesis of ceramics can be done by sol-gel, co-precipitation, the precursor solution technique, and the hydrothermal

process (Jha et al., 2003; Liu et al., 2007; Masingbon et al., 2008). To meet the need for titanates and niobates in the capacitor sector, Pechini developed the Pechini process (Pechini et al., 1967). Utilising modified Pechini techniques, also known as the citrate gel process or the amorphous citrate gel process, a variety of ceramic oxide powders are created. The process includes combining solutions of a metal precursor with an organic polyfunctional acid, such as citric acid, glycine, tartaric acid, or glycerol, that has at least one hydroxyl and one carboxylic acid group. The metal and polycarboxylic acid thereby acquire complexity. After the water has entirely evaporated from the solutions by heating, a very viscous resin is produced. The powder is then produced by heating, crushing, and finally calcining the resin's organic components. The glycine gel nitrate technique is one of the combustion processes used to create ceramic particles. An extremely viscous mass that is produced after the evaporation of a metal nitrate and glycine solution is ignited to produce the powder (Chick et al., 1990). The complexing agent glycine prevents the metal ions from precipitating as the water evaporates. Both the carboxylic end and the amino group end of the compound can form complexes with cations. Glycine serves as a fuel for the process ignition step in addition to its other essential functions when it is oxidised by nitrate ions. Extreme caution must be taken at this point since the reactions that happen during ignition are very explosive. Typically, only a little bit at a time ought to be lit. In contrast to the Pechini method, the creation of a loose mass of extremely fine crystalline powder after ignition under well-controlled conditions negates the need for grinding. The powder's unusually small particle size and crystalline structure are thought to be the result of its brief exposure to high temperatures during the ignition stage. This means that very fine,

chemically homogenous powder can be produced using the glycine gel nitrate approach for a fair price. Both simple and complicated oxides, such as manganites, chromites, ferrites, and oxide superconductors, have been synthesised using it.

1.11. Dielectric properties of metal oxide

1.11.1 Capacitors

The capacitor resembles a miniature rechargeable battery, capable of storing energy in the form of an electrical charge, resulting in a potential difference across its plates. Its primary design consists of two or more parallel conductive plates, separated by air or high-quality insulating materials such as mica, ceramic, plastic waxed paper, or electrolytic gel (utilized in electrolytic capacitors). These capacitors are engineered for swift energy discharge when needed. The dielectric refers to the insulating layer situated between the plates of a capacitor. Due to the potential difference between the conductors and the alignment of charges within the dielectric, a static electric field emerges across it. As a result, positive charges tend to accumulate on one capacitor plate, while negative charges do the same on the other plate. This electrostatic field is responsible for storing the energy in the capacitor. In Figure 1.12, The functioning of a parallel plate capacitor can be observed in a circuit, as well as the distribution of charges within the dielectric material.

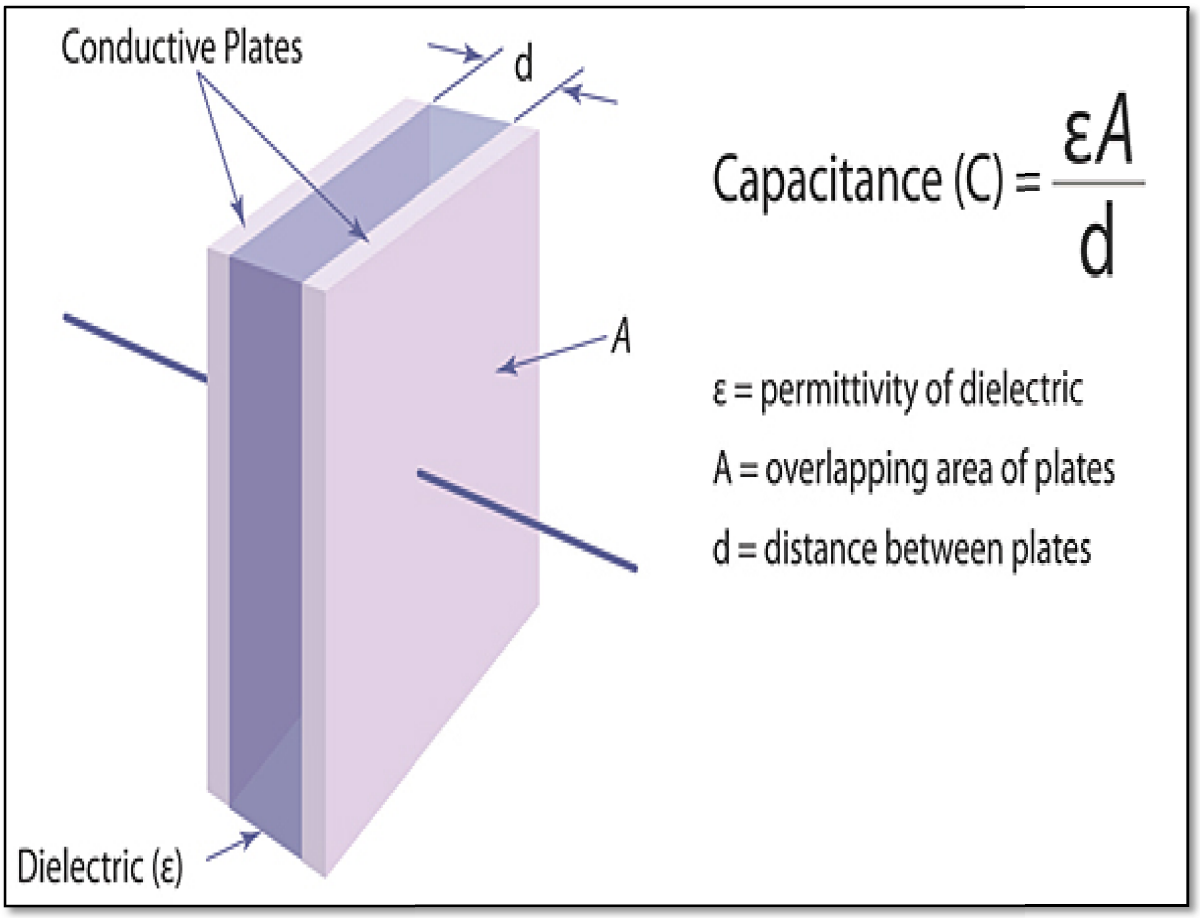

Fig. 1.12. Shows parallel plate capacitors in circuit, including the alignment of charges in the dielectric material [110]

The capacitance of the parallel plate capacitor is shown in the equation:

$$C = \varepsilon_0 A/d \qquad (1.2)$$

where, ε_0 (= 8.854 x 10^{-12} F/m) is the permittivity of free space. In the pursuit of miniaturization and higher capacitance in a specific area, selecting materials with a higher

dielectric constant is preferred when designing embedded capacitors. This choice allows for the achievement of greater capacitance within the given space.

1.11.2. Dielectric materials

Ceramic materials, also referred to as dielectric materials, serve as efficient electrical insulators, and they exhibit unique dielectric and electrical properties. These materials are neither electrically conductive nor completely unresponsive to the applied electric field (E). Due to the influence of the electric field, there is a partial Polarization of material as depicted in Fig. 1.13.

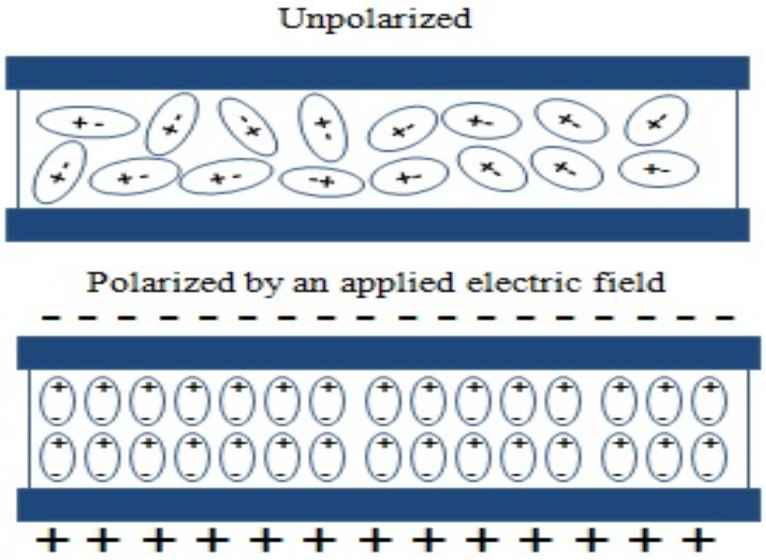

Fig.1.13. The polarized and non-polarized plates of an applied electric field .[111]

So for, the system occupies an electrical dipole moment (P) .These dipole moment found per unit volume is called polarization. The moment is proportional to the electric field (E) and the polarization is proportional to the applied field [112] show in equation

$$P = n\chi eE \qquad (1.3)$$

Where, χ_e is the dielectric susceptibility; n is a constant that describes the dielectric ability to form dipoles [113]. Since the dielectric susceptibility χ_e is equal to $(\varepsilon_r\text{-}1)$, where ε_r is the relative permittivity, the polarization will be [114].

$$P = \varepsilon_o E (\varepsilon_r - 1) \qquad (1.4)$$

It is well-established that the field encountered by a molecule within a dielectric, situated between plates of a charged capacitor, is significantly enhanced compared to the externally applied field. This phenomenon is closely related to the polarization exhibited by the surfaces of the dielectric material. The actual field of a molecule is called the local field (E_{loc}). The dipole moment for a molecule by the local field is given by [115].

$$P_{mol} = \alpha' E_{loc} \qquad (1.5)$$

where, P_{mol} is a moment and α' shows the polarizability of the molecule. For dielectrics containing N molecules per unit volume, the total dipole moment or polarization is:

$$P = N \alpha' E_{loc} \qquad (1.6)$$

Substituting Equation (1.4) in Equation (1.5) gives

$$\chi_e = (\varepsilon_r\text{-}1) = P/ \varepsilon_o E_{loc} = N \alpha' E_{loc}/ \varepsilon_o E \qquad (1.7)$$

The presence of a dielectric substance reduces various effective polarization processes, including electronic polarization, orientation (dipolar) polarization, space charge

polarization, and atomic or ionic polarization. The net polarization P of the dielectric material, and is given as:

$$P = P_{\text{electronic}} + P_{ionic} + P_{molecular} + P_{interfacial}$$

1.12. Electronic Polarization

Electronic polarization is a phenomenon observed in all dielectric materials. When a single atom is subjected to an electric field (E), its electrons surrounding the nucleus undergo a minute shift in the direction of the positive electrode, while the nucleus experiences a slight shift towards the negative electrode, and the atom acquires a dipole moment (P) so that:

$$P = \alpha' E \qquad (1.8)$$

Upon removing the electric field, the electrons and nuclei swiftly revert to their original distributions, causing the polarization to vanish. Due to the relatively minor charge displacement associated with electronic polarization, the total amount of polarization is significantly smaller when compared to other polarization mechanisms. [116]

1.12.1. Orientation Polarization

The arrangement of the individual atoms within the molecule, if the system is made up of heteronuclear (non-symmetrical) molecules, may be such that the molecule itself has a permanent dipole moment. H_2O, HCl, CH_3Br, HF, and $C_2H_5(NO_2)$ are among examples. The two hydrogen atoms that have a net positive charge are on one side of the oxygen atom that has a net negative charge because the covalent bonds between the hydrogen and oxygen atoms in H_2O are directed. The molecule will align with its positive side facing the negative electrode and its negative side facing the positive electrode when exposed to an electric field

[116]. Not all molecules composed of different atoms are necessarily polar. For instance, CO_2 is considered non-polar since the carbon and oxygen atoms form a straight-line arrangement, with carbon in the middle. On the other hand, H_2O is polar because its atoms are arranged in a triangular fashion (see table 1.3) [117]. Among polarizations, orientation polarization proves to be more advantageous than electronic polarization, primarily because it allows for greater charge displacement in relatively large molecules compared to the differences between electrons and nuclei in individual atoms [116]. However, in solid materials, molecules are usually closely bound, limiting the occurrence of orientation polarization. In contrast, this type of polarization is more significant in liquids and gases.

As the temperature decreases, the effectiveness of orientation polarization increases due to the influence of thermal vibrations, which tend to randomize the molecular orientation. Consequently, the resulting dielectric constant becomes temperature-dependent [117].

1.12.2. Space Charge Polarization

Space charges originate from various processes such as cosmic radiation, thermal degradation, or entrapment within the substance after its creation, leading to the generation of random charges [116].

1.12.3. Atomic or Ionic Polarization

Atomic polarization refers to the phenomenon where atoms (or ions) within a crystal structure undergo displacement when subjected to an electric field. This field exerts a force on the atoms, causing a stretching of the bonds that connect them, resulting in a change in the overall molecular moment. The extent and nature of this polarization effect depend on

various factors, including the specific crystal structure, the presence of solid solutions, and other relevant coefficients [116]

Table 1.2. Shows polarization mechanism of dielectric materials

Polarization Mechanism					
Type of polarization	**No E field** (E=0)	**Local Field E** (E≠0)	**Case where it is Observed**	**Frequency range where it is predominant**	**Strength of Polarization**
Electronic Polarization	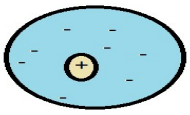	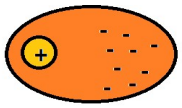	Neutral atoms	~ 10^{15} Hz	Very weak
Atomic or Ionic polarization	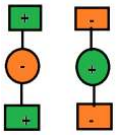	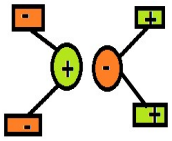	Ionic species	10^{12} to 10^{13} Hz	Strong
Molecular or Orientation or Dipolar Polarization		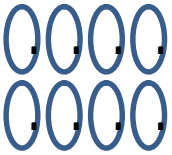	Molecules with permanent dipole moment	10^{11} to 10^{12} Hz	Weak
Interfacial					

Polarization	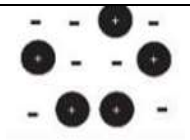	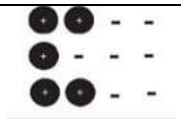	Heterogeneous Systems	10^{-3} to 10^{3} Hz	Very strong

1.13. Dielectric constant

The relative permittivity or dielectric constant of a material defines both its capacity to store charges and the duration of its polarization. When an electric field is applied between two metal flat plates, one plate becomes positively charged, and the other becomes negatively charged. The material situated between these conductive plates undergoes polarization due to the influence of the electric field. The polarizability of the material is compared to that of the vacuum between the plates using the relative dielectric constant (k) [116].

$k' = k$ Material / k vacuum (1.9)

In other references; the relative permittivity is quoted as (ε_r), while, ε_0 is defined as the permittivity of the free space and ε is the permittivity of the dielectric material. The permittivity terms (ε_r, ε_0, ε) will be used according to Equation (1.10).

$$\varepsilon_r = \varepsilon / \varepsilon_0 \quad (1.10)$$

Electrical insulator applications use materials having a low dielectric constant. For charge storage and other purposes, capacitors use materials with a high dielectric constant. For embedded capacitors to obtain high energy density in a given space and further miniaturisation, high dielectric constant materials are preferred. In an alternating field, dielectric constant (k) can be expressed as

$$k = \varepsilon' - j\varepsilon'' = \varepsilon_0\varepsilon_r - j\varepsilon'' \quad (1.11)$$

where, ε' is real dielectric constant, and ε'' is imaginary dielectric constant. Real dielectric constant (ε') is directly related to the material. The dielectric constant should ideally be unaffected by changes in frequency, temperature, voltage, or time. Each polarisation mechanism does, however, have an own relaxation frequency. Depending on the type of material, the values of dielectric materials can also fluctuate with temperature, bias, impurity, and crystal structure to varying degrees [118]**.**

1.14. Dielectric loss

A measure of the energy loss of the dielectric during ac operation, dielectric loss is a material feature of the dielectric. Distortion, dipolar, interfacial, and conduction losses all contribute to dielectric loss. Dielectric loss is expressed as the loss tangent (tan δ) or Dissipation factor (D_f), and is defined as:

$$tan\ \delta = \varepsilon''\varepsilon' + \sigma 2\pi f\varepsilon \quad (1.12)$$

where, ε', ε'' are real and imaginary parts of dielectric permittivity, σ is electrical conductivity of the material and f is frequency. Energy loss (W) which is defined as the energy dissipated in a dielectric material is proportional to the loss tangent, and is expressed as:

$$W \approx \pi\varepsilon' E2ftan\delta \quad (1.13)$$

where E is electric field strength and f is frequency. Therefore, a low dielectric loss is preferred in order to reduce the energy dissipation and signal losses, particularly for high frequency applications. Generally, a dissipation factor under 0.1% is considered to be quite low and 5% is high [118]

1.15. Impedance

Impedance spectroscopy stands out as a highly effective and powerful method for investigating the electrical properties of various materials and their interactions with electrically conducting electrodes. This technique allows for a comprehensive examination of both bound and mobile charge movements within the bulk or interfacial regions of solid or liquid materials. Its versatility extends to the study of ionic, semiconducting, mixed electronic-ionic, dielectric (even insulating), charge carrier migration across grain and grain boundaries, and other related phenomena.The process of impedance spectroscopy involves the application of a single frequency of voltage or current to the interface of the material under study. Subsequently, an analog or digital circuit is utilized to measure crucial parameters such as phase shift, amplitude, and the real and imaginary components of the resulting current at that specific frequency. Through this approach, researchers gain valuable insights into the electrical behavior and characteristics of the materials, which can have significant implications across various scientific and engineering domains. At the core of this essential technique lies the analysis of the alternating current (AC) response of a system when subjected to a sinusoidal disturbance. By calculating the impedance as a function of the perturbation's frequency, valuable insights can be obtained. Impedance spectroscopy spectra usually fall into two distinct categories.

The first category pertains to the material itself, encompassing crucial properties such as conductivity, dielectric constant, mobilities of charges, equilibrium concentrations of charged species, and bulk generation-recombination rates. These factors provide valuable

information about the electrical characteristics and behavior of the material. The second category focuses on the electrode-material interface, involving key aspects like adsorption-reaction rate constants, interface capacitance, and diffusion coefficient of neutral species within the electrode. Understanding these parameters is vital for comprehending the interactions and dynamics between the material and the electrically conducting electrode. Through this approach, researchers can discern and quantify various electrical phenomena and properties, enabling deeper insights into the nature of materials and their interface interactions. The outcomes of impedance spectroscopy analysis contribute significantly to diverse fields, spanning from material science to electrochemistry and beyond. Impedance spectroscopy has become a pivotal aspect of modern electronic automation, with significant and intentional contributions to various fields. The integration of sophisticated automatic experimental equipment allows for precise measurements and analysis of the frequency response to small-amplitude AC signals, typically falling within the frequency range of about 10^-4 to >10^-6 Hz. This data is seamlessly interfaced with computer chips, finding applications in diverse industries such as industrial quality control for paints, emulsions, electroplating, thin-film technology, materials fabrication, engine mechanical performance, corrosion assessment, and more. The impedance itself is characterized by two components: a real component (Z') and an imaginary component (Z''). These values can be obtained through experimental measurements. Depending on the material under study and the hypothesized processes, researchers can construct an electrical equivalent circuit comprising elements like capacitors, inductors, resistors, and other relevant components. This equivalent circuit allows for a more comprehensive understanding of the electrical behavior

and properties of the material. To further explore and interpret the impedance data, mathematical transforms are employed, providing related values and insights into the material's characteristics. The ability to analyze impedance spectra and extract valuable information has propelled advancements in numerous scientific and industrial endeavors, making impedance spectroscopy an indispensable tool in the realm of electronic automation and beyond. A few oxide compounds with their dielectric constant, are listed below [119].

Table 1.3. High dielectric constant of few oxide compounds

S.No.	**Compound**	**Dielectric constant**	**Reference**
1.	$CaCu_{2.70}Mg_{0.30}Ti_4O_{12}$	340000	[120]
2.	$Bi_{2/3}Cu_3Ti_4O_{12}$	29000	[121]
3.	$Ba(Fe_{0.5}Nb_{0.5})O_3$-$Bi_{0.2}Y_{2.8}Fe_5O_{12}$	30000	[122]
4.	$Ba_{0.75}Sr_{0.25}TiO_3$	24000	[123]
5.	$CaCu_3Ti_4O_{12}$	20000	[92]
6.	$K_{0.5}Na_{0.5}NbO_3$	20000	[124]
7.	$Bi_{1.5}ZnNb_{1.5}O_7$	10,000	[125]
8.	$0.5BaTiO_3–0.5Bi_{2/3}Cu_3Ti_4O_{12}$	43459	[126]
9.	$Ba_6Y_2Ti_4O_{17}$	1500	[127]
10.	Eu_2CuO_4	5000	[128]

11.	$0.5Bi_{2/3}Cu_3Ti_4O_{12}$- $0.5Bi_3LaTi_3O_{12}$	13900	[129]
12.	$CaCu_{2.9}Zn_{0.1}Ti_4O_{12}$	5971	[130]
13.	$Y_{2/3}Cu_3Ti_{3.95}In_{0.05}O_{12}$	5068	[131]
14	$Bi_{0.5}Na_{0.5}TiO_3$	5000	[132]
15.	$(Ba_{0.95}Ca_{0.05})$ $(Ti_{0.96}Zr_{0.04})O_3$	3910	[133]

The real and imaginary parts of the complex dielectric constant are represented as:

$$\varepsilon' = -Z''/\omega C (Z'^2 + Z''^2) \quad (1.14)$$

$$\varepsilon'' = -Z'/\omega C (Z'^2 + Z''^2) \quad (1.15)$$

The real and imaginary parts of complex electric modulus are represented as:

$$M' = \omega CZ'' \quad (1.16)$$

$$M'' = \omega CZ' \quad (1.17)$$

The loss tangent is given as

$$\tan\delta = \varepsilon'/\varepsilon'' = M''/M' \quad (1.18)$$

the radial frequency, ω, is given as

$$\omega = 2\pi f \quad (1.19)$$

with f being the frequency and the vacuum capacitance C is given in equation (1.20)

$$C = \varepsilon A/d \quad (1.20)$$

with A is the area of the electrode and d is the thickness of the dielectric layer.

1.16. Electrical conductivity:

Electrical resistivity is equal to the reciprocal of electrical conductivity, also known as specific conductance. It shows how well a substance can carry electric current. The SI unit for electrical conductivity is the siemens per metre (S/m), which is often represented by the Greek character (sigma). Conductivity and resistance are important characteristics of materials that determine how much resistance a typical material has to current flow. Electrical resistance and conductance are complementary broad qualities that determine an object's resistance to an electric current.

1.17. Aim of study:

The persistent drive to shrink electronic devices, including cell phones, digital cameras, laptops, computers, and TVs, is widely acknowledged. There is an ongoing pursuit to create capacitor materials with both a substantial dielectric constant and minimal loss, particularly for deployment in microelectronics, microwave technology, memory systems, and energy storage devices based on capacitance. CCTO emerges as a promising candidate to fulfill these demands owing to its exceptional thermal stability and remarkable dielectric constant and is stable between 100—600 K in the low frequency region 10^2-10^5 Hz.

1) This work focuses on the study of the synthesis, characterization and the effect of different cationic substitutions such as Zn^{2+}, Mg^{2+} and Ni^{2+}at Cu site and Ge^{4+} at Ti^{4+} site in $Bi_{2/3}Cu_3Ti_4O_{12}$ on the dielectric properties and electrical behavior as a function of temperature and frequency.

2) With a view to separate the contributions of grains and grain boundaries the microstructure of the different ceramics will also be studied towards electrical and dielectric properties at various temperature and frequency.

3) In order to obtain good quality of $Bi_{2/3}Cu_3Ti_4O_{12}$ electro-ceramic by the conventional solid-state method, the semi-wet method and ball mill route, the effect of sintering temperature and sintering duration will be studied. In addition, an effort will be made to get high dielectric constant and low dielectric loss BCTO ceramic suitable for use as capacitor material showing high thermal stability and independent in frequency.

The objective of the present investigation is to synthesize the following BCTO and its isomorphs by different methods indicated in the parenthesis:

(i) $Bi_{2/3}Cu_3Ti_4O_{12}$ (BCTO) by semi-wet route

(ii) $Bi_{2/3}Cu_{2.95}Mg_{0.05}Ti_4O_{12}$ (BCMgTO-0.05) by semi-wet route

(iii) $Bi_{2/3}Cu_{2.90}Mg_{0.10}Ti_4O_{12}$ (BCMgTO-0.1) by semi-wet route

(iv) $Bi_{2/3}Cu_{2.80}Mg_{0.20}Ti_4O_{12}$ (BCMgTO-0.2) by semi-wet route

(v) $Bi_{2/3}Cu_{2.95}Ni_{0.05}Ti_4O_{12}$ (BCNTO-0.05) synthesized by semi-wet route

(vi) $Bi_{2/3}Cu_{2.90}Ni_{0.10}Ti_4O_{12}$ (BCNTO-0.1) synthesized by semi-wet route

(vii) $Bi_{2/3}Cu_{2.80}Ni_{0.20}Ti_4O_{12}$ (BCNTO-0.2) synthesized by semi-wet route

(viii) $Bi_{2/3}Cu_{2.95}Zn_{0.05}Ti_4O_{12}$ (BCZTO-0.05) by semi-wet route

(ix) $Bi_{2/3}Cu_{2.90}Zn_{0.10}Ti_4O_{12}$ (BCZTO-0.1) by semi-wet route

(x) $Bi_{2/3}Cu_{2.80}Zn_{0.20}Ti_4O_{12}$ (BCZTO-0.2) by semi-wet route

(xi) $Bi_{2/3}Cu_3Ti_{3.95}Ge_{0.05}O_{12}$ (BCTGO-0.05) synthesized by semi-wet route

(xii) $Bi_{2/3}Cu_{2.95}Zn_{0.05}Ti_{3.95}Ge_{0.05}O_{12}$ (BCZTGO-0.05) synthesized by semi-wet route

These ceramics will be characterized by different physiochemical techniques. The powder X-ray diffraction will be recorded to study the crystal structure and single phase formation of the ceramic. Scanning electron micrographs of the ceramics will be recorded to study the

surface morphology and transmission electron micrographs will be obtained to determine their particle size. The purity and stoichiometry of each of grain and grain-boundary region will be assessed by the energy dispersive X-ray spectroscopy (EDX). With a view to obtain high dielectric constant and low dielectric loss the dielectric and electrical properties will be studied as a function of temperature as well as frequency. In addition, a correlation between dielectric behavior and those of microstructure and defect structure will be established.

References:

[1] Zhang, W.B., Yu, X., Wang, C.L., Sun, H.J., Hsieh, I.F., Li, Y., Dong, X.H., Yue, K., Van Horn, R., and Cheng, S.Z. (2014). Molecular nanoparticles are unique elements for macromolecular science: From "nanoatoms" to giant molecules. *Macromolecules*, 47(4), 1221-1239.

[2] Grassian, V.H. (2008). When size really matters: size-dependent properties and surface chemistry of metal and metal oxide nanoparticles in gas and liquid phase environments. *The Journal of Physical Chemistry C*, 112(47), 18303-18313.

[3] Long, N.V., Yang, Y., Thi, C.M., Van Minh, N., Cao, Y., and Nogami, M. (2013). The development of mixture, alloy, and core-shell nanocatalysts with nanomaterial supports for energy conversion in low-temperature fuel cells. *Nano Energy*, 2(5), 636-676.

[4] Vest, M.A., Lui, K.C., and Kung, H.H. (1989). Catalytic decomposition of methanol on ZnO single-crystal surfaces at low and near-atmospheric pressures. *Journal of Catalysis*, 120(1), 231-255.

[5] Krotee, P., Rodriguez, J.A., Sawaya, M.R., Cascio, D., Reyes, F.E., Shi, D., Hattne, J., Nannenga, B.L., Oskarsson, M.E., Philipp, S., and Griner, S. (2017). Atomic structures of fibrillar segments of hIAPP suggest tightly mated β-sheets are important for cytotoxicity. *Elife*, 6, 19273.

[6] Nakka, L., Molinari, J.E., and Wachs, I.E. (2009). Surface and bulk aspects of mixed

oxide catalytic nanoparticles: oxidation and dehydration of CH_3OH by polyoxometallates. *Journal of the American Chemical Society*, 131(42),15544-15554.

[7] Goldstein, A.N., Echer, C.M. and Alivisatos, A.P. (1992). Melting in semiconductor nanocrystals. *Science*, 256(5062), 1425-1427.

[8] Reed, M.A., Frensley, W.R., Matyi, R.J., Randall, J.N., and Seabaugh, A.C. (1989). Realization of a three-terminal resonant tunneling device: The bipolar quantum resonant tunneling transistor. *Applied physics letters*, 54(11), 1034-1036.

[9] Alivisatos, A.P. (1996). Semiconductor clusters, nanocrystals, and quantum dots. *science*, 271(5251), 933-937.

[10] Raimondi, F., Scherer, G.G., Kötz, R., and Wokaun, A. (2005). Nanoparticles in energy technology: examples from electrochemistry and catalysis. *Angewandte Chemie International Edition*, 44(15), 2190-2209.

[11] Kerker M. (1985). Effect of optical constants on calculated values of surface-enhanced Raman scattering. *Journal of the Optical Society of America B*, 2(8), 1327, 1985.

[12] Hassan, M.S., Amna, T., Kim, H.Y., and Khil, M.S. (2013). Enhanced bactericidal effect of novel CuO/TiO_2 composite nanorods and a mechanism thereof. *Composites Part B: Engineering*, 45(1), 904-910.

[13] Li, Y., Qian, F., Xiang, J., and Lieber, C.M. (2006). Nanowire electronic and optoelectronic devices. *Materials today*, 9(10), 18-27.

[14] Wang, G., Shen, X., Yao, J., and Park, J. (2009). Graphene nanosheets for enhanced lithium storage in lithium ion batteries. *Carbon*, *47*(8), pp.2049-2053.

[15] Xu R. (2003) Measuring explained variation in linear mixed effects models. *Statistics*

in Medicine, 22(22), 3527–3541.

[16] Yousef, A., Barakat, N.A., Amna, T., Al-Deyab, S.S., Hassan, M.S., Abdel-Hay, A., and Kim, H.Y. (2012). Inactivation of pathogenic Klebsiella pneumoniae by CuO/TiO_2 nanofibers: A multifunctional nanomaterial via one-step electrospinning. *Ceramics International*, 38(6), 4525-4532.

[17] Butler, S.Z., Hollen, S.M., Cao, L., Cui, Y., Gupta, J.A., Gutiérrez, H.R., Heinz, T.F., Hong, S.S., Huang, J., Ismach, A.F., and Johnston-Halperin, E. (2013). Progress, challenges, and opportunities in two-dimensional materials beyond graphene. *ACS nano*, 7(4), 2898-2926.

[18] Khan M. F., Hameedullah M., Ansari A. H., Ahmad E., Lohani M.B., Khan R. H. Alam M.M., Khan W., Husain F. M., and Ahmad I. (2008). Flower-shaped ZnO nanoparticles synthesized by a novel approach at near-room temperatures with antibacterial and antifungal properties**.** *International Journal of Nanomedicine*, 1,60–66.

[19] Mani P., Srivastava R., and Strasser P. (2011). Dealloyed binary PtM_3 (M = Cu, Co, Ni) and ternary $PtNi_3M$ (M = Cu, Co, Fe, Cr) electrocatalysts for the oxygen reduction reaction: Performance in polymer electrolyte membrane fuel cells. *Journal of Power Sources*, vol. 196(2), 666–673.

[20] Pudukudy M., Hetieqa A., and Yaakob Z. (2014) Synthesis, characterization and photocatalytic activity of annealingdependent quasi spherical and capsule like ZnO nanostructures. *Applied Surface Science*, 319(1), 221–229.

[21] F. S. Ke. (2009). One-step fabrication of CuO nanoribbons array electrode and its excellent lithium storage performance. *Electrochimica Acta*, 54(24), 5825–5829.

[22] Pang H., Gao F., and Lu Q. (2009). Morphology effect on antibacterial activity of cuprous oxide. *Chemical Communications*, 9, 1076–1078, 2009.

[23] Hoffmann M. R., Martin S. T., Choi W., and Bahnemann D. W. (1995). Environmental Applications of Semiconductor Photocatalysis. *Chemical Reviews*, 95(1), 69–96.

[24] Burda C., Chen X., Narayanan R., and El-Sayed M. A. (2005). Chemistry and properties of nanocrystals of different shapes. *Chemical Reviews*, 105(4), 1025-1032.

[25] T. Hyeon T., Lee S. S., Park J., Chung Y., and Na H. B. (2001) Synthesis of highly crystalline and monodisperse maghemite nanocrystallites without a size-selection process. *Journal of the American Chemical Society*, 123(51), 12798–12801.

[26] Rana S., Rawat J., Sorensson M. M., and Misra R. D. K. (2006). Antimicrobial function of Nd^{3+}-doped anatase titania-coated nickel ferrite composite nanoparticles: A biomaterial system. *Acta Biomaterialia*, 2(4), 421–432.

[27] Pudukudy M., and Yaakob Z. (2014). Facile solid state synthesis of ZnO hexagonal nanogranules with excellent photocatalytic activity. *Applied Surface Science*, 292, 520–530.

[28] Sathishkumar P., Sweena R., Wu J. J., and Anandan S. (2011). Synthesis of CuO-ZnO nanophotocatalyst for visible light assisted degradation of a textile dye in aqueous solution. *Chemical Engineering Journal*, 171(1), 136–140.

[29] Yanagimoto T. , Yu Y. T., and Kaneko K. (2012). Microstructure and CO gas sensing property of Au/SnO_2 core-shell structure nanoparticles synthesized by precipitation method and microwave-assisted hydrothermal synthesis method. *Sensors and Actuators, B: Chemical*, 166, 31–35.

[30] Christy A. J., and Umadevi M. (2013). Novel combustion method to prepare octahedral NiO nanoparticles and its photocatalytic activity," *Materials Research Bulletin*, vol. 48(10), 4248–4254.

[31] Gordon T., Perlstein B., Houbara O., Felner I., Banin E., and Margel S. (2011). Synthesis and characterization of zinc/iron oxide composite nanoparticles and their antibacterial properties. *Colloids and Surfaces A: Physicochemical and Engineering Aspects*, 374(1–3), 1–8.

[32] Abe, M., and Uchino, K. (1974). X-ray study of the deficient perovskite $La_{23}TiO_3$. *Materials Research Bulletin,* 9, 147–155.

[33] Ahmadipour, M., Ain, M.F., and Ahmad, Z.A. (2016). A Short Review on Copper Calcium Titanate (CCTO) Electroceramic: Synthesis, Dielectric Properties, Film Deposition, and Sensing Application. *Nano-Micro Letter,* 8, 291–311.

[34] Ali, R., and Yashima, M. (2005). Space group and crystal structure of the Perovskite $CaTiO_3$ from 296 to 1720K. *Journal of Solid State Chemistry* 178, 2867–2872.

[35] Molina-García A., M., and V. Rees, N. (2016). Effect of catalyst carbon supports on the oxygen reduction reaction in alkaline media: a comparative study. *RSC Advances* 6, 94669–94681.

[36] Ali R, and Yashima M. (2005). Space group and crystal structure of the Perovskite $CaTiO_3$ from 296 to 1720K. *Journal of Solid State Chemistry.* 178(9), 2867–2872.

[37] Bai Y., Cheng Z-Y, Bharti V., Xu H.S., and Zhang Q.M. (2000). High-dielectric-constant ceramicpowder polymer composites. Applied Physics Letter, 76(25):3804–3806.

[38] Balamurugaraj P., Suresh S., Koteeswari P., and Mani P. (2013). Growth, optical, mechanical, dielectric and photoconductivity properties of L-proline succinate NLO single crystal. *Journal of Material Chemistry and Physics*, 1(1), 4–8.

[39] Boonlakhorn J., and Thongbai P. (2020). Dielectric properties, nonlinear electrical response and microstructural evolution of $CaCu_3Ti_{4-x}Sn_xO_{12}$ ceramics prepared by a double ball-milling process. *Ceramics International*, 46(4), 4952–4958.

[40] Cabuk S., Akkus H., and Mamedov A.M. (2007). Electronic and optical properties of KTaO3: Ab initio calculation. *Physica B: Condensed Matter.* 394(1): 81–85.

[41] Cain M.G., and Stewart M. (2014). Losses in Piezoelectrics via Complex Resonance Analysis. In: Cain MG, editor. Characterisation of Ferroelectric Bulk Materials and Thin Films. *Dordrecht: Springer Netherlands. (Springer Series in Measurement Science and Technology),* 233–242.

[42] Carrasco J., Illas F., Lopez N., Kotomin E.A., Zhukovskii Y.F., Evarestov R.A., Mastrikov Y.A., Piskunov S., and Maier J. (2006). First-principles calculations of the atomic and electronic structure of F centers in the bulk and on the (001) surface of $SrTiO_3$. *Physical Review B,* 73(6), 064106.

[43] Chandler C.D., Roger C., and Hampden-Smith M.J. (1993). Chemical aspects of solution routes to perovskite-phase mixed-metal oxides from metal-organic precursors. Chem Review, 93(3):1205–1241.

[44] Chaudhuri A, and Mandal K. (2012). Enhancement of ferromagnetic and dielectric properties of lanthanum doped bismuth ferrite nanostructures. Materials Research Bulletin, 47(4), 1057–1061.

[45] Chu M.W., Ganne M., Caldes M.T., Brohan L. (2002). X-ray photoelectron spectroscopy and high resolution electron microscopy studies of Aurivillius compounds: $Bi_{4-x}La_xTi_3O_{12}$ (x= 0, 0.5, 0.75, 1.0, 1.5, and 2.0). *Journal of applied physics*, 91(5), 3178–3187.

[46] Affleck, L., and Leach, C. (2005). Microstructures of $BaTiO_3$ based PTC thermistors with Ca, Sr and Pb additions. *Journal of the European Ceramic Society*, 25(12), 3017-3020

[47] Ahmed, M. A., Ateia, E., Salah, L. M., and El-Gamal, A. A. (2005). Structural and electrical studies on La^{3+} substituted Ni–Zn ferrites. *Materials chemistry and physics*, 92(2-3), 310- 321.

[48] Akhtar, M. N., Hussain, T., Khan, M. A., and Ahmad, M. (2018). Structural, magnetic, dielectric and high frequency response of synthesized rare earth doped bismuth nano garnets (BIG). *Results in Physics*, 10, 784-793.

[49] Azcondo, M. T., de Paz, J. R., Boulahya, K., Ritter, C., García-Alvarado, F., and Amador, U. (2015). Complex magnetic behaviour of $Sr_2CoNb_{1-x}Ti_xO_6$ ($0 \leq x \leq 0.5$) as a result of a flexible microstructure. *Dalton Transactions*, 44(8), 3801-3810.

[50] Ashima, A., Sanghi, S., Agarwal, A., and Reetu, R. (2012). Rietveld refinement, electrical properties and magnetic characteristics of Ca-Sr substituted barium hexaferrites. *Journal of alloys and compounds*, 513, 436-444.

[51] Anupama, A. V., Keune, W., and Sahoo, B. (2017). Thermally induced phase transformation in multi-phase iron oxide nanoparticles on vacuum annealing. *Journal of Magnetism and Magnetic Materials*, 439, 156-166.

[52] Arora, A., and Narang, S. B. (2016). Structural and dielectric properties of co-substituted Mtype barium hexaferrite. *Journal of Materials Science: Materials in Electronics,* 27(10), 10157-10162.

[53] Ahmed, M. A., El Hiti, M. A., El Nimr, M. K., and Amer, M. A. (1996). The ac electrical conductivity for Co-substituted Sb Ni ferrites. *Journal of magnetism and magnetic materials*, 152(3), 391-395.

[54] Ahmed, T. T., Rahman, I. Z., and Rahman, M. A. (2004). Study on the properties of the copper substituted Ni Zn ferrites. *Journal of Materials Processing Technology*, 153, 797-803.

[55] Almeida, R. M., Paraguassu, W., Pires, D. S., Correa, R. R., and de Araujo Paschoal, C. W. (2009). Impedance spectroscopy analysis of $BaFe_{12}O_{19}$ M-type hexaferrite obtained by ceramic method. *Ceramics International*, 35(6), 2443-2447.

[56] Ahmed, A. I., Siddig, M. A., Mirghni, A. A., Omer, M. I., and Elbadawi, A. A. (2015). Structural and optical properties of $Mg_{1-x}Zn_xFe_2O_4$ nano-ferrites synthesized using coprecipitation method. *Advances in Nanoparticles*, 4(2), 45.

[57] Ashiq, M. N., Asi, A. S., Farooq, S., Najam-ul-Haq, M., & Rehman, S. (2017). Magnetic and electrical properties of M-type nano-strontium hexaferrite prepared by sol-gel combustion method. *Journal of Magnetism and Magnetic Materials*, 444, 426-431.

[58] Anbarasu, V., Gazzali, P. M., Karthik, T., Manigandan, A., and Sivakumar, K. (2013). Effect of divalent cation substitution in the magnetoplumbite structured $BaFe_{12}O_{19}$ system. *Journal of Materials Science: Materials in Electronics*, 24(3), 916-926.

[59] Bhalla, A.S., Guo, R. and Roy, R. (2000). The perovskite structure – a review of its role in ceramic science and technology. *Materials Research Innovations*, 4, 3–26.

[60] Bobnar, V., Hrovat, M., Holc, J., and Kosec, M. (2009). All-ceramic lead-free percolative composite with a colossal dielectric response. *Journal of the European Ceramic Society*, 29(4), 725-729.

[61] Yang X. N. , Qu N. G., Bin Wang H., Huang B. B., and Wei J. Y. (2006). A study of La-doped Bi_2Ti2O_7 nanocrystals prepared by chemical solution deposition technique. *Materials Letters*, 60(23), 2886–2888.

[62] Bibes M., and Barthélémy A. (2007). Oxide spintronics, *IEEE Transactions on Electron Devices*, 54(5), 1003–1023.

[63] Davies P. K., Wu H., Borisevich A. Y., Molodetsky I. E., and Farber L. (2008). Crystal chemistry of complex perovskites: New cation-ordered dielectric oxides. *Annual Review of Materials Research*, 38, 369–401.

[64] Banerjee S., Kim D. I., Robinson R. D., Herman I. P., Mao Y., and Wong S. S. (2006). Observation of Fano asymmetry in Raman spectra of SrTiO3 and $Ca_x\ Sr_{1-x}TiO_3$ perovskite nanocubes, *Applied Physics Letters*, 89(22), 1–4.

[65] Mao Y., Park T. J., and Wong S. S. (2005). Synthesis of classes of ternary metal oxide nanostructures. *Chemical Communications*, 46, 5721–5735.

[66] Rostami, M., Moradi, M., Alam, R. S., and Mardani, R. (2016). Characterization of magnetic and microwave absorption properties of multi-walled carbon nanotubes/Mn-Cu-Zr substituted strontium hexaferrite nanocomposites. *Materials Research Bulletin*, 83, 379-386.

[67] Roshanaei, K. (2017). Controlled synthesis and photocatalytic activities of barium

hexaferrite nanoparticles and examine decolorization methyl orange on liver of rats. *Journal of Materials Science: Materials in Electronics*, 28(6), 4537-4544.

[68] Respaud, M., Broto, J. M., Rakoto, H., Fert, A. R., Thomas, L., Barbara, and Osuna, J. (1998). Surface effects on the magnetic properties of ultrafine cobalt particles. *Physical Review B*, 57(5), 2925.

[69] Singh, L., Rai, U. S., and Mandal, K. D. (2013). Dielectric, modulus and impedance spectroscopic studies of nanostructured $CaCu_{2.70}Mg_{0.30}Ti_4O_{12}$ electro-ceramic synthesized by modified sol–gel route. *Journal of Alloys and Compounds*, 555, 176-183.

[70] Soomro, S. A., Gul, I. H., Khan, M. Z., Naseer, H., and Khan, A. N. (2017). Dielectric properties evaluation of $NiFe_2O_4$/MWCNTs nanohybrid for microwave applications prepared via novel one step synthesis. *Ceramics International*, 43(5), 4090-4095.

[71] Salame, P. H., Prakash, O., and Kulkarni, A. R. (2016). Colossal dielectric constant and extremely low loss in T-type $La_2CuO_{4-\delta}$ ceramics. Ceramics International, 42(11), 13207-13214.

[72] Singh, L., Yadava, S. S., Woo, W. S., Rai, U. S., Mandal, K. D., Sin, B. C., and Lee, Y. (2016). Structural, impedance, and modulus spectroscopic studies on $Y_{2/3}Cu_3Ti_{3.95}In_{0.05}O_{12}$ polycrystalline material prepared by flame synthesis method. *Applied Spectroscopy Reviews*, 51(7-9), 735-752.

[73] Söderlind, F., Selegård, L., Nordblad, P., Uvdal, K., and Käll, P. O. (2009). Sol–gel synthesis and characterization of polycrystalline $GdFeO_3$ and $Gd_3Fe_5O_{12}$ thin films. *Journal of sol-gel science and technology*, 49(2), 253-259.

[74] Koinuma H. (2005). Chemistry and electronics of oxides from carbon dioxide to

perovskite," *Thin Solid Films*, 486(1–2), 2–10.

[75] Stefaniuk, I., Matkovskii, A., Rudowicz, C., Suchocki, A., Wilamowski, Z., Lukasiewicz, T., and Galazka, Z. (2006). Electron paramagnetic resonance studies of cobalt and rare-earth impurity ions in $YAlO_3$. *Journal of Physics: Condensed Matter*, 18(19), 4751.

[76] Schenck, J. F. (2005). Physical interactions of static magnetic fields with living tissues. *Progress in biophysics and molecular biology*, 87(2-3), 185-204.

[77] Song, Q., and Zhang, Z. J. (2004). Shape control and associated magnetic properties of spinel cobalt ferrite nanocrystals. *Journal of the American Chemical Society*, 126(19), 6164-6168.

[78] Sivakumar, M., Gedanken, A., Zhong, W., Du, Y. W., Bhattacharya, D., Yeshurun, Y., and Felner, I. (2004). Nanophase formation of strontium hexaferrite fine powder by the sonochemical method using $Fe(CO)_5$. *Journal of Magnetism and Magnetic Materials*, 268(1- 2), 95-104.

[79] Carrasco, J., Illas, F., Lopez, N., Kotomin, E.A., Zhukovskii, Y.F., Evarestov, R.A., Mastrikov, Y.A., Piskunov, S. and Maier, J. (2006). First-principles calculations of the atomic and electronic structure of F centers in the bulk and on the (001) surface of $SrTiO_3$. *Physical Review B*, *73*(6), 064106.

[80] Singhal, S., Namgyal, T., Singh, J., Chandra, K., & Bansal, S. (2011). A comparative study on the magnetic properties of $MFe_{12}O_{19}$ and $MAlFe_{11}O_{19}$ (M= Sr, Ba and Pb) hexaferrites with different morphologies. *Ceramics International*, 37(6), 1833-1837.

[81] Sankaranarayanan, V. K., Pankhurst, Q. A., Dickson, D. P. E., & Johnson, C. E. (1993). Ultrafine particles of barium ferrite from a citrate precursor. *Journal of magnetism and*

magnetic materials, 120(1-3), 73-78.

[82] Sudakar, C., Subbanna, G. N., and Kutty, T. R. N. (2003). Wet chemical synthesis of multicomponent hexaferrites by gel-to-crystallite conversion and their magnetic properties. J*ournal of magnetism and magnetic material*s, 263(3), 253-268.

[83] Shafi, K. V. P. M., & Gedanken, A. (1999). Sonochemical approach to the preparation of barium hexaferrite nanoparticles. *Nanostructured Materials*, 12(1-4), 29-34.

[84] Sharma, P., Rocha, R. A., De Medeiros, S. N., and Paesano Jr, A. (2007). Structural and magnetic studies on barium hexaferrites prepared by mechanical alloying and conventional route. *Journal of Alloys and Compounds*, 443(1-2), 37-42.

[85] Shirk, B. T., and Buessem, W. R. (1969). Temperature dependence of Ms and K 1 of $BaFe_{12}O_{19}$ and $SrFe_{12}O_{19}$ single crystals. *Journal of Applied Physic*s, 40(3), 1294-1296.

[86] Sharma, S., Yadav, S. S., Singh, M. M., and Mandal, K. D. (2014). Impedance spectroscopic and dielectric properties of nanosized $Y_{2/3}Cu_3Ti_4O_{12}$ ceramic. J*ournal of Advanced Dielectrics*, 4(4), 1450030.

[87] Singh, L., Yadava, S. S., Sin, B. C., Rai, U. S., Mandal, K. D., and Lee, Y. (2016). Comparative Dielectric and Ferroelectric Characteristics of $Bi_{0.5}Na_{0.5}TiO_3$, $CaCu_3Ti_4O_{12}$, and $0.5Bi_{0.5}Na_{0.5}TiO_3$–$0.5CaCu_3Ti_4O_{12}$ Electroceramics. *Journal of Electronic Materials*, 45(6), 2662-2672.

[88] Soman, V. V., Nanoti, V. M., and Kulkarni, D. K. (2013). Dielectric and magnetic properties of Mg–Ti substituted barium hexaferrite. Ceramics International, 39(5), 5713-5723.

[89] Moreira M. L. (2008). Photoluminescence of barium titanate and barium zirconate in

multilayer disordered thin films at room temperature. *Journal of Physical Chemistry A*, vol. 112(38), 8938–8942.

[90] Carrasco J., Illas F., Lopez N., Kotomin E.A., Zhukovskii Y.F., Evarestov R.A., Mastrikov Y.A., Piskunov S., and Maier J. (2006). First-principles calculations of the atomic and electronic structure of F centers in the bulk and on the (001) surface of $SrTiO_3$. *Physical Review B.* 73(6):064106.

[91] Chandler C.D., Roger C., Hampden-Smith M.J. (1993). Chemical aspects of solution routes to perovskite-phase mixed-metal oxides from metal-organic precursors. *Chemical Review*, 93(3):1205–1241.

[92] Adams T.B., Sinclair D.C. and West A.R. (2002). Giant barrier layer capacitance effects in $CaCu_3Ti_4O_{12}$ ceramics. *Advanced Materials*, *14*(18), 1321-1323.

[93] Chu M-W, Ganne M, Caldes MT, and Brohan L. (2002). X-ray photoelectron spectroscopy and high resolution electron microscopy studies of Aurivillius compounds: $Bi_{4-x}La_xTi_3O_{12}$ (x= 0, 0.5, 0.75, 1.0, 1.5, and 2.0). *Journal of applied physics*, 91(5), 3178–3187.

[94] Ball C. J., Begg B. D., Cookson D. J., Thorogood G. J. , and Vance E. R. (1998) Structures in the System $CaTiO_3/SrTiO_3$. *Journal of Solid State Chemistry*, 139(2), 238–247.

[95] Boulahya K., Muñoz Gil D., Hassan M. , García Martin S., and Amador U. (2017). Structural and microstructural characterization and properties of new phases in the Nd-Sr-Co-(Fe/Mn)-O system as air-electrodes in SOFCs. *Dalton Transactions*, 46(4), 1283–1289.

[96] Amow G., Au J., and Davidson I. (2006). Synthesis and characterization of $La_4Ni_{3-x}Co_xO_{10\pm\delta}$ ($0.0 \leq x \leq 3.0$, $\Delta x = 0.2$) for solid oxide fuel cell cathodes. *Solid State Ionics*, vol.

177(19-25), 1837–1841.

[97] Li X., and Benedek N. A. (2015). Enhancement of ionic transport in complex oxides through soft lattice modes and epitaxial strain. *Chemistry of Materials*, 27(7), 2647–2652.

[98] Kim, J., Yin, X., Tsao, K.C., Fang, S. and Yang, H. (2014). $Ca_2Mn_2O_5$ as oxygen-deficient perovskite electrocatalyst for oxygen evolution reaction. *Journal of the American Chemical Society*, *136*(42),14646-14649.

[99] Shin, Y. and Rondinelli, J.M. (2020). Pressure effects on magnetism in $Ca_2Mn_2O_5$-type ferrites and manganites. *Physical Review B*, *102*(10),104426.

[100] Mao, P., Wang, J., Liu, S., Zhang, L., Zhao, Y. and He, L. (2019). Grain size effect on the dielectric and non-ohmic properties of $CaCu_3Ti_4O_{12}$ ceramics prepared by the sol-gel process. *Journal of Alloys and Compounds*, 778, 625-632.

[101] Yang, L., Song, L., Li, Q. and Zhang, T. (2021). Dielectric properties and electrical response of yttrium-doped $Bi_{2/3}Cu_3Ti_4O_{12}$ ceramics. *Journal of Advanced Dielectrics*, *11*(01), 2150007.

[102] Rani, S., Ahlawat, N., Sangwan, K.M., Rani, S., Punia, R. and Malik, J. (2018). Structural investigation and giant dielectric response of $CaCu_3Ti_4O_{12}$ ceramic by Nd/Zr co-doping for energy storage applications. *Journal of Materials Science: Materials in Electronics*, 29, 10825-10833.

[103] Subramanian, M.A., Li, D., Duan, N., Reisner, B.A. and Sleight, A.W. (2000). High dielectric constant in $ACu_3Ti_4O_{12}$ and $ACu_3Ti_3FeO_{12}$ phases. *Journal of Solid State Chemistry*, 151(2), 323-325.

[104] Kai, C., Wei, L., Yun-Fei, L., Peng, B., Xiao-Mei, L. and Jin-Song, Z. (2004).

Investigation of the size effect on the giant dielectric constant of $CaCu_3Ti_4O_{12}$ ceramic. *Chinese Physics Letters*, *21*(9), 1815.

[105] Li, M., Feteira, A., Sinclair, D.C. and West, A.R. (2006). Influence of Mn doping on the semiconducting properties of $CaCu_3Ti_4O_{12}$ ceramics. *Applied physics letters*, *88*(23).

[106] Bueno, P.R., Tararan, R., Parra, R., Joanni, E., Ramirez, M.A., Ribeiro, W.C., Longo, E. and Varela, J.A. (2009). A polaronic stacking fault defect model for $CaCu_3Ti_4O_{12}$ material: an approach for the origin of the huge dielectric constant and semiconducting coexistent features. *Journal of Physics D: Applied Physics*, *42*(5), 055404.

[107] Li, W. and Schwartz, R.W. (2006). ac conductivity relaxation processes in $CaCu_3Ti_4O_{12}$ ceramics: Grain boundary and domain boundary effects. *Applied physics letters*, *89*(24).

[108] Tan, Y.Q., Zhang, J.L., Hao, W.T., Chen, G., Su, W.B. and Wang, C.L. (2010). Giant dielectric-permittivity property and relevant mechanism of $Bi_{2/3}Cu_3Ti_4O_{12}$ ceramics. *Materials Chemistry and Physics*, 124(2-3),1100-1104.

[109] Yang, Z., Liang, P., Yang, L., Shi, P., Chao, X. and Yang, Z. (2015). Synthesis, dielectric properties of $Bi_{2/3}Cu_3Ti_4O_{12}$ ceramics by the sol–gel method. *Journal of Materials Science: Materials in Electronics*, 26,1959-1968.

[110] Grove, T.T., Masters, M.F. and Miers, R.E. (2005). Determining dielectric constants using a parallel plate capacitor. *American journal of physics*, *73*(1), 52-56.

[111] Morozhenko, V., Maslov, V. and Kachur, N. (2018). Manifestation of the Faraday effect in non-polarized light under optical resonance conditions. *Optics Communications*, *426*, 423-426.

[112] Pandey, S., Kumar, V., Sharma, V.K. and Mandal, K.D. (2020). Effect of doping metal ions on microstructural evolution and dielectric behaviors of $CaCu_3Ti_4O_{12}$ ceramics synthesized by semi-wet route. *Materials Chemistry and Physics*, 253, 123384.

[113] Claros, M., Setka, M., Jimenez, Y.P. and Vallejos, S. (2020). AACVD synthesis and characterization of iron and copper oxides modified ZnO structured films. *Nanomaterials*, 10(3), 471.

[114] Jaiswar, S. and Mandal, K.D. (2017). Evidence of enhanced oxygen vacancy defects inducing ferromagnetism in multiferroic CaMn7O12 manganite with sintering time. *The Journal of Physical Chemistry C*, 121(36), 19586-19601.

[115] Thakur, S., Rai, R., Bdikin, I. and Valente, M.A. (2016). Impedance and modulus spectroscopy characterization of Tb modified $Bi_{0.8}A_{0.1}Pb_{0.1}Fe_{0.9}Ti_{0.1}O_3$ ceramics. *Materials Research*, 19, 1-8.

[116] Daud, N., Mohamed, J.J., Mohamad, H., Warikh, A.R.M., Noh, M.Z. and Nor, M.A.A.M. (2019). The effect Ca content on thermal properties of Ca1-xCu3Ti4O12-x ceramics. *AIP Conference Proceedings*, 2068(1), 20023.

[117] Liu, L., Ren, S., Liu, J., Han, F., Zhang, J., Peng, B., Wang, D., Bokov, A.A. and Ye, Z.G. (2019). Localized polarons and conductive charge carriers: understanding $CaCu_3Ti_4O_{12}$ over a broad temperature range. *Physical Review B*, 99(9), 094110.

[118] Slimani, Y., Unal, B., Hannachi, E., Selmi, A., Almessiere, M.A., Nawaz, M., Baykal, A., Ercan, I. and Yildiz, M. (2019). Frequency and dc bias voltage dependent dielectric properties and electrical conductivity of $BaTiO_3SrTiO_3/(SiO_2)_x$ nanocomposites. *Ceramics International*, 45(9),11989-12000.

[119] Robertson, J. (2004). High dielectric constant oxides. *The European Physical Journal-Applied Physics*, 28(3), 265-291.

[120] Singh, L., Rai, U.S. and Mandal, K.D. (2013). Dielectric, modulus and impedance spectroscopic studies of nanostructured $CaCu_{2.70}Mg_{0.30}Ti_4O_{12}$ electro-ceramic synthesized by modified sol–gel route. *Journal of alloys and compounds*, 555,176-183.

[121] Gautam, P., Khare, A., Sharma, S., Singh, N.B. and Mandal, K.D. (2016). Characterization of $Bi_{2/3}Cu_3Ti_4O_{12}$ ceramics synthesized by semi-wet route. *Progress in Natural Science: Materials International*, 26(6), 567-571.

[122] Yang, H., Bai, L., Lin, Y., Wang, F. and Wang, T. (2017). Magneto-dielectric laminated Ba ($Fe_{0.5}Nb_{0.5}$) O_3-$Bi_{0.2}Y_{2.8}Fe_5O_{12}$ composites with high dielectric constant and high permeability. *Ceramics International*, 43(3), 2903-2909.

[123] Huang, J., Cao, Y., Hong, M. and Du, P., 2008. Ag–Ba0. 75Sr0. 25TiO3 composites with excellent dielectric properties. *Applied Physics Letters*, *92*(2).

[124] Ahn, C.W., Lee, S.Y., Lee, H.J., Ullah, A., Bae, J.S., Jeong, E.D., Choi, J.S., Park, B.H. and Kim, I.W. (2009). The effect of K and Na excess on the ferroelectric and piezoelectric properties of K0. 5Na0. 5NbO3 thin films. *Journal of Physics D: Applied Physics*, 42(21), 215304.

[125] Du, H. and Yao, X. (2003). Effects of Sr substitution on dielectric characteristics in Bi1. 5ZnNb1. 5O7 ceramics. *Materials Science and Engineering: B*, 99(1-3),.437-440.

[126] Khare, A., Yadava, S., Gautam, P., Mukhopadhyay, N. and Mandal, K. (2017). Effect of sintering on the dielectric properties of 0.5 BaTiO-0.5 BiCuTiO nanocomposite synthesized by solid state route. *Journal of Materials Science: Materials in*

Electronics, 28(7), 5523-5530.

[127] SundaráYadava, S. (2016). Dielectric, ferroelectric and magnetic properties of hexagonal Ba 6 Y 2 Ti 4 O 17 (BYTO) perovskite derived from semi wet route. *RSC Advances*, 6(106),104941-104948.

[128] Salame, P., Drai, R., Prakash, O. and Kulkarni, A.R. (2014). IBLC effect leading to colossal dielectric constant in layered structured Eu2CuO4 ceramic. *Ceramics International*, 40(3), 4491-4498.

[129] Gautam, P., Yadava, S.S., Khare, A. and Mandal, K.D. (2017). Dielectric and magnetic studies of 0.5 Bi2/3Cu3Ti4O12-0.5 Bi3LaTi3O12 nano-composite ceramic synthesized by semi-wet route. *Ceramics International*, 43(3), 3133-3139.

[130] Jaiswal, V., Rastogi, R.B., Kumar, R., Singh, L. and Mandal, K.D. (2014). Tribological studies of stearic acid-modified CaCu 2.9 Zn 0.1 Ti 4 O 12 nanoparticles as effective zero SAPS antiwear lubricant additives in paraffin oil. *Journal of Materials Chemistry A*, 2(2), 375-386.

[131] Singh, L., Yadava, S.S., Woo, W.S., Rai, U.S., Mandal, K.D., Sin, B.C. and Lee, Y. (2016). Structural, impedance, and modulus spectroscopic studies on $Y_{2/3}Cu_3Ti_{3.95}In_{0.\ 05}O_{12}$ polycrystalline material prepared by flame synthesis method. *Applied Spectroscopy Reviews*, 51(7-9), 735-752.

[132] Yang, Z., Liu, B., Wei, L. and Hou, Y. (2008). Structure and electrical properties of $(1-x)Bi_{0.5}Na_{0.5}TiO_{3-x}Bi_{0.5}K_{0.5}TiO_3$ ceramics near morphotropic phase boundary. *Materials Research Bulletin*, 43(1), 81-89.

[133] Yang, S., Zhang, H., Zhang, S.W. and Zhang, B.P. (2011). Electrical properties tailoring in Ni-particle-dispersed $(Ba_{0.95}Ca_{0.05})(Ti_{0.96}Zr_{0.04})O_3$ composites. *Materials Chemistry and Physics*, *126*(3), 729-733.